DESIGN, FABRICATION AND CHARACTERIZATION OF LIQUID-SOLID MICROELECTROMECHANICAL DC-CONTACT SWITCHES

A THESIS

SUBMITTED TO THE MATERIALS SCIENCE AND

NANOTECHNOLOGY PROGRAM

OF THE GRADUATE SCHOOL OF ENGINEERING AND SCIENCE

OF BILKENT UNIVERSITY

IN PARTIAL FULFILLMENT OF THE REQUIREMENTS

FOR THE DEGREE OF

MASTER OF SCIENCE

By

Engin Çağatay

August, 2012

I certify that I have read this thesis and that in my opinion it is fully adequate, in scope and in quality, as a thesis for the degree of Master of Science.

Assist. Prof. Dr. Necmi Bıyıklı(Advisor)

I certify that I have read this thesis and that in my opinion it is fully adequate, in scope and in quality, as a thesis for the degree of Master of Science.

Assist. Prof. Dr. Aykutlu Dana

I certify that I have read this thesis and that in my opinion it is fully adequate, in scope and in quality, as a thesis for the degree of Master of Science.

Assist. Prof. Dr. Ali Kemal Okyay

Approved for the Graduate School of Engineering and Science:

Prof. Dr. Levent Onural
Director of the Graduate School

ABSTRACT

DESIGN, FABRICATION AND CHARACTERIZATION OF LIQUID-SOLID MICROELECTROMECHANICAL DC-CONTACT SWITCHES

Engin Çağatay
M.S. in Materials Science and Nanotechnology
Supervisor: Assist. Prof. Dr. Necmi Bıyıklı
August, 2012

From critical applications such as life support systems and massive data communication centers to every day necessities like mobile phones and street lighting, people depend on the performance of electrical switches. Today, the vast majority of electrical switches are of solid-state semiconductor type. They are fast, with nanosecond response times, have the advantage of being produced by CMOS-compatible microfabrication processes, and unlike their major competitor counterparts, i.e., microelectromechanical systems (MEMS) switches, they do not suffer from mechanical contact issues like contact bounce, stiction, or contact degradation, due to the absence of solid-to-solid mechanical contacts. Therefore, electrical switches exhibit extremely long life times with superior reliability performance. However, they have a high ON-state resistance of 2-6 Ω, low open-state impedance on the order of 10^5-10^7 Ω, and show relatively low power-handling capabilities. In addition, their temperature and radiation-sensitive performance, limits their range of operating environment.

The major counterpart switching technology, solid-to-solid DC-contact MEMS switches, on the other hand, transmit current when the two surfaces, namely dimple and contact pad, make contact. Although MEMS switches show very good RF performance, the required solid-to-solid contact is often quite non-ideal. This stems from the fact that the two contact surfaces have certain micro or nano-scale roughness including nano-scale asperities and thus cannot conform perfectly onto each other. Consequently, the actual contact area is only a small fraction of the apparent one. These devices suffer from mechanical problems such as switch bouncing, microwelding, adhesion and contact degradation, and as a result show degraded switching performance over time with long-term reliability issues.

At this point, an alternative switching technology might be the proposal of liquid-to-solid MEMS (LS-MEMS) switches using movable liquid metal droplets. This promising concept enables electrical switches with higher isolation and lower insertion loss, much like conventional solid-solid MEMS switches. Moreover, since they do not have fragile moving solid parts, LS-MEMS switches potentially do not suffer from mechanical fatigue problems increased contact resistance and stiction/adhesion problems.

Our aim in this study is to design and fabricate LS-MEMS switches, whereby we can characterize and examine the actuation of metallic liquid droplets, namely eutectic Ga-In (EGaIn), Gallium Indium Tin alloy (Galinstan), and mercury (Hg) using electrowetting on dielectric (EWOD) principle. We have investigated the effect of different actuation electrode geometries like rectangular, interdigitated fingers and crescent-shaped electrodes on the droplet actuation. With the application of 30-100 V voltage difference across the actuation electrode and the ground electrode, the metallic liquid droplets were observed to be actuated. With further optimization, LS-MEMS device structures demonstrated in this work might have potential applications as alternative high-performance electrical switches.

Keywords: Liquid-solid microelectromechanical system (LS-MEMS), electrowetting-on-dielectric (EWOD), microfabrication, Galinstan, eutectic Ga-In, DC-contact switch, actuation, metallic liquid droplet.

ÖZET

SIVI-KATI MİKROELEKTROMEKANİK DC-KONTAK ANAHTARLARIN TASARIMI, ÜRETİMİ VE ÖLÇÜMÜ

Engin Çağatay
Malzeme Bilimi ve Nanoteknoloji, Yüksek Lisans
Tez Yöneticisi: Yard. Doç. Dr. Necmi Bıyıklı
Ağustos, 2012

İnsanlar, yaşam destek sistemleri ve veri iletişim merkezleri gibi kritik öneme sahip uygulamalardan telefon ve sokak aydınlatması gibi günlük ihtiyaçlara kadar çeşitli alanlarda elektronik anahtarların başarımına muhtaçtır. Günümüzde, bu anahtarların ezici çoğunluğunda yarı-iletken temelli katı hal teknolojisi kullanılmaktadır. Anahtarlama hızı nano saniyelerle ölçülen bu anahtarlar, CMOS uyumlu olma avantajının yanı sıra, katı-katı mekanik kontaklara sahip olmadıkları için, Mikroelektromekanik-Sistem (MEMS) anahtarlardan farklı olarak kontak sıçraması, yapışması ve zamanla kontak direncinin artması gibi sorunlarla karşılaşmazlar. Bu nedenle de, yüksek güvenirliğin yanında, oldukça uzun çalışma ömrüne sahiptirler. Tüm bu avantajlarına rağmen, 2-6 Ω gibi yüksek iletken durum direncine, 10^5-10^7 Ω aralığında düşük bir iletken durum sönümlenmesine ve görece düşük güç-taşıma kabiliyetine sahiptirler. Bunlara ek olarak, başarımlarının sıcaklığa ve radyasyona hassas olması, çalışma koşullarına sınırlamalar getirmektedir.

Katı hal elektronik anahtarlar dışında başlıca diğer anahtarlama teknolojisi olan katı-katı DC-kontak MEMS anahtarlar, gelen akımı anahtarın iki katı metalik yüzeyi bir araya gelip temas sağladığında aktarır. MEMS anahtarlar çok iyi RF başarımı sağlasa da, gerekli olan katı-katı yüzey teması genelde idealden uzaktır. Bunun nedeni, iki temas yüzeyinin de sahip olduğu mikro ve nano boyuttaki pürüzlülükten dolayı, temas sırasında birbirlerine tam olarak değememesidir. Sonuç olarak, gerçek temas alanı, görünenin sadece küçük bir kısmına karşılık gelmektedir. Bu tür anahtarlar, anahtar sıçraması, mikrokaynak, yapışma ve temas bozulması gibi mekanik sorunlara maruz kalırlar ve bunun sonucunda, uzun dönemli güvenirlik sorunlarının yanında zamanla azalan bir anahtarlama başarımı gösterirler.

Bu noktada alternatif bir anahtarlama teknolojisi olarak, hareket eden sıvı metal damlaları kullanan sıvı-katı MEMS anahtar yapıları önerilebilir. Bu ümit veren yenilikçi aygıt mimarisi, geleneksel katı-katı MEMS anahtarlara benzer olarak, yüksek yalıtım ve düşük araya sokma yitimi sağlamaktadır. Ayrıca, hareket eden hassas katı parçaları olmadığından sıvı-katı MEMS anahtarlar mekanik yorulma, yüksek temas direnci ve yapışma gibi sorunlardan potansiyel olarak etkilenmezler.

Bu çalışmanın amacı, sıvı-katı MEMS anahtarlar tasarlamak, üretmek ve daha sonra, yalıtkan üzerinde elektrikle ıslatma (electrowetting-on-dielectric, EWOD) ilkesini kullanarak, ötektik Ga-In (EGaIn), Galyum İndiyum Kalay alaşımı (Galinstan), ve civa (Hg) sıvı metal damlalarının harekete geçirilmesi kabiliyetlerini ölçmek ve incelemektir. Bu çalışmada kare, birbirine geçmiş parmaklar ve hilal gibi değişik harekete geçirme elektrotu şekillerinin, damlacıkların harekete geçme özellikleri üzerindeki etkisi araştırılmıştır. Harekete geçirme elektrotuyla toprak elektrotu arasında 30-100 V voltajın uygulanmasıyla, sıvı metal damlacıklarının hareket ettiği gözlemlenmiştir. Bu çalışmada sunulan cihaz yapıları, alternatif yüksek-başarımlı anahtarların geliştirilmesinde potansiyel kullanım alanı bulabilir.

Anahtar sözcükler: Sıvı-katı mikroelektromekanik sistem (MEMS), yalıtkan üzerinde elektrikle ıslatma (EWOD), mikrofabrikasyon, Galinstan, ötektik Ga-In, DC kontak anahtar, harekete geçirmek, metal sıvı damlacığı.

To my family

and

Nazlı Deniz

Acknowledgement

I would like to express my deepest gratitude to my supervisor Assist. Prof. Dr. Necmi Bıyıklı for his precious guidance, advice, criticism, encouragement, and insight throughout the development of this work. I would like to thank specially Assist. Prof. Dr. Aykutlu Dana and Assist. Prof. Dr. Ali Kemal Okyay for being in my thesis committee and sharing their useful comments.

I also wish to thank Bilkent UNAM for the interdisciplinary research environment and state-of-the-art equipment it provided to me throughout the research.

I would also thank all Bıyıklı research group members including Çağla Özgit-Akgün, İnci Dönmez and Alican Noyan, and UNAM colleagues who have contributed my research and made it a joy for me including Alper Yeşilyurt, Temmuz Ceyhan, Mustafa Kemal Ruhi, Ahmet Deniz Usta, Feyza Oruç, Gürkan Polat, Adem Saraç, Yasin Damgacı, Levent Aygün, Fatih Bilge Atar, Deniz Kocaay, Fikret Piri and Semih Yaşar.

Special appreciation and gratitude are also to my family for their endless love, constant support, great patience and extensive encouragement throughout my whole life. Also, I would like to express my deepest appreciation to Kahyaoğlu family for their great support and patience. Finally, the words are not enough to express my appreciation to my dearest, Nazlı Deniz, I cannot even imagine a life without her.

Contents

List of Figures

List of Tables

List of Symbols and Abbreviations

ALD	: Atomic Layer Deposition
BOE	: Buffered Oxide Etchant
CAH	: Contact Angle Hysteresis
CMOS	: Complementary Metal Oxide Semiconductor
CPW	: Co-Planar Waveguide
DI	: Deionized
EDL	: Electric Double Layer
EGaIn	: Eutectic Gallium Indium
EWOD	: Electrowetting-On-Dielectric
Galinstan	: Gallium Indium Tin alloy
GDS	: Graphic Database System
ICP	: Inductively Coupled Plasma
IR	: Image Reversal
ITO	: Indium Tin Oxide
LoC	: Lab-On-a-Chip
LS-MEMS	: Liquid-Solid Microelectromechanical Systems
MEMS	: Microelectromechanical Systems
NP	: Nanoparticle
PECVD	: Plasma Enhanced Chemical Vapor Deposition
PR	: Photoresist
RF	: Radio Frequency
RPM	: Revolutions Per Minute
SAM	: Self-Assembled Monolayer
SEM	: Scanning Electron Microscope
sccm	: Standard Cubic Centimeters per Minute
TMA	: Trimethylaluminum
TMMMA	: Perfluoro Methacrylate Methyl Methacrylate
UCF	: UNAM Cleanroom Facility
UV	: Ultraviolet

Chapter 1

Introduction

Electrowetting-on-dielectric (EWOD) is the phenomenon in which the wetting properties of a liquid are modified by the influence of an applied electric field. Devices used for this purpose consist of a metal electrode, the droplet to be actuated, and a dielectric layer between them (Figure 1.1(a)). With the application of voltage between the metal electrode and the electrically conducting liquid droplet, the droplet spreads over the dielectric. Moreover, if there is more than one electrode under the dielectric, the droplet moves towards the electrode on which the voltage is applied (Figure 1.1(b)). Using EWOD effect, both conducting and non-conducting liquids can be actuated [1]. Electrowetting finds potential use in several different fields and disciplines, such as lab-on-a-chip (LoC) systems, electronic displays, and electrical switches [2], [3], [4].

Switches with mercury-wetted solid contacts were first developed in the 1940s in order to benefit from longer lifetime and lower switching noise in addition to other advantages of electromechanical switches. Hermetically packaged in hydrogen environment to avoid mercury oxidation, they contained a movable and a fixed metallic contact in a sealed glass envelope containing a pool of doped mercury. When the switches were actuated magnetically, they demonstrated bounce-free operation, low contact resistance ($< 50\ m\Omega$), long life (over 10^9 cycles), and fast rise time [5]. Mercury-wetted switches were heavily commercialized and extensively used in telephony and other low-signal high-bandwidth applications [5].

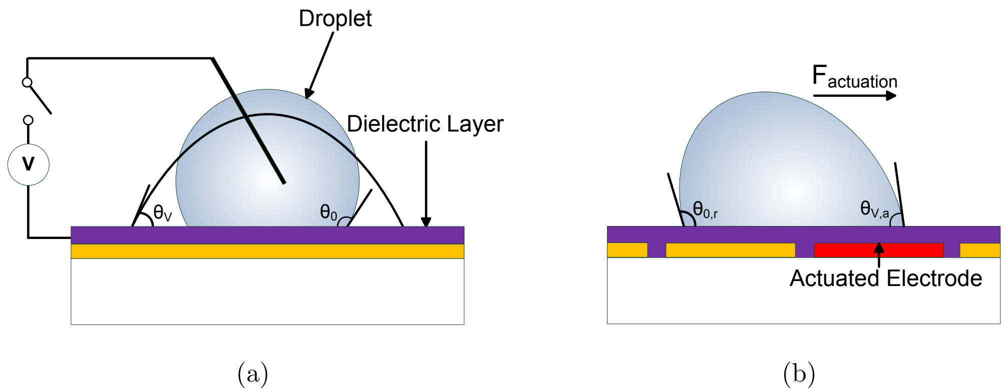

Figure 1.1: (a) EWOD device consisting of a metal electrode, the droplet to be actuated, and a dielectric layer in between. (b) Actuation of a droplet on a device with more than one electrode.

However, these switches were slow, sensitive to gravity, and posed environmental hazard, as the quantity of mercury contained in each switch was significant. Recent studies showed that these problems can be overcome by alternative switch designs as in the work of Sen et al. They report switches with 60μs switch-on latency and with stability up to 16g acceleration [6].

Mainly two basic types of EWOD devices have been studied in the literature: open setup and closed setup devices, shown schematically in Figure 1.2(a) and Figure 1.2(b), respectively. The main difference between the two is that the closed setup has a continuous ground electrode on the top plate, whereas in the open setup, the ground electrode is on the same wafer as the actuation electrodes. A summary of the previous efforts carried out in this field is presented in Table 1.1. Potassium chloride solution (KCl), deionized (DI)-water, and mercury (Hg) droplets have been used and different electrode materials have been utilized including chromium (Cr), titanium (Ti), and gold (Au).

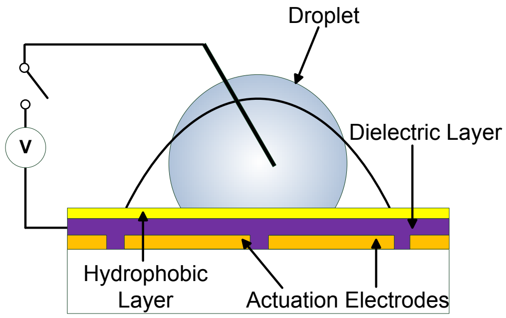

(a)

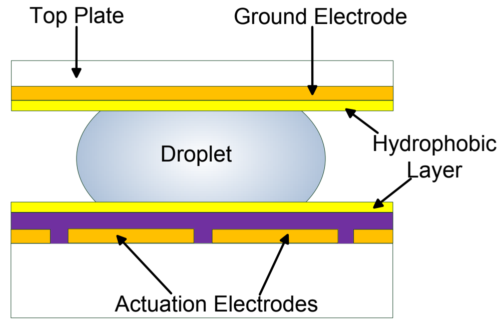

(b)

Figure 1.2: (a) An open setup EWOD device. (b) A closed setup EWOD device.

Table 1.1: Summary of previous work on EWOD-based droplet actuation

Group	**Setup**	**Droplet**	$\mathbf{V}_{\text{act}}$	**Electrodes**	**Dielectric**
Rajabi [2]	Closed	KCl sol'n	55V	Cr	Parylene C
Chang et al. [7]	Open	DI-water	$<$ 15V	Au	Al_2O_3 (ALD)
Chang et al. [8]	Open	DI-water	90V	Cr	Polyimide
Chen & Peroulis [9]	Open	Mercury	110V	Ti/Au/Ti	SiO_2 (PECVD)

1.1 Problem Statement

Solid-solid DC contact microelectromechanical (MEMS) switches transmit current when the two surfaces, namely dimple and contact pad, as shown in Figure 1.3(a), make contact. Although MEMS switches show very good RF performance, the required solid-to-solid contact is often quite non-ideal. This stems from the fact that the two contact surfaces have certain micro- or nano-scale roughnesses including nano-scale asperities, and thus cannot conform perfectly on each other. Consequently, the actual contact area is only a small fraction of the apparent one (Figure 1.3(b)). This limits the power handling ability of the switch since it forces the switched current to transverse through a very limited contact area [9].

Another consequence of the non-ideal contacts in conventional MEMS switches

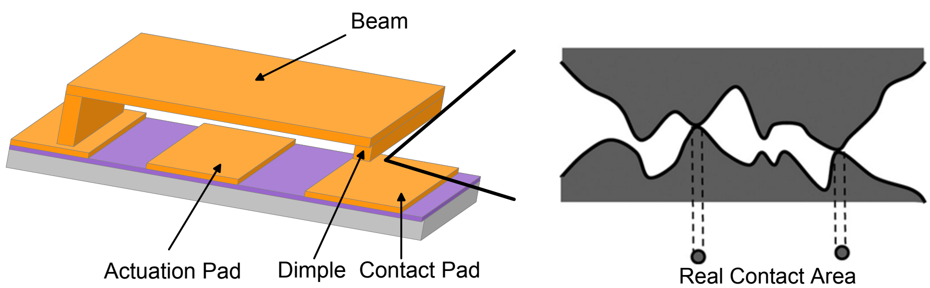

(a) (b)

Figure 1.3: (a) Schematic representation of a solid-solid DC contact MEMS switch. (b) Micro- or nano-scale roughnesses including nano-scale asperities which make harder for the two surfaces to conform perfectly on each other [10].

is the contact resistance. Although the contact resistance decreases with increasing contact force, there exists a threshold level of the force, which is the minimum contact force required for getting a stable and reproducible contact resistance. Forces higher than the threshold level further decrease the contact resistance, but only to a smaller extent. Table 1.2 shows the minimum contact force necessary to realize a stable contact resistance for various metals and contact resistance at the minimum contact force. Both the contact resistance and the minimum contact force are lower for soft materials compared to hard materials. This is due to the adaptation of contact surfaces to each other by elastoplastic deformation, which results in a sufficiently large effective contact area [11].

Evenmore, conventional MEMS switches also suffer from problems such as switch bouncing, welding, adhesion, and contact degradation. Patton et al. conducted studies of hot-switched gold (Au) contacts using a micro/nanoadhesion apparatus as a switch simulator. The instrument used a ball-on-flat configuration and Au was coated onto balls and wafers, which were then used in experiments. At low current (1-10 μA), they observed slightly higher contact resistance, asperity creep, high adhesion after rapid switching, switch bouncing, and reasonable durability. On the other hand, at high current (1-10 mA) observations include: slightly lower contact resistance, melting, no measurable adhesion, less tendency for switch bouncing, necking of contacts, and poor reliability and durability due

Table 1.2: Minimum contact force to achieve a stable microcontact resistance for different metals and contact resistance at the minimum contact force [11]

Material	**Minimum contact force [μN]**	**Contact resistance [mΩ]**
gold (Au)	50-100	70-200
'fine-gold' (AuCuCd)	200	50-80
'hard-gold' (AuNi, 5%)	300-450	<100
gold-palladium (AuPd)	200-2000	500-3000
palladium (Pd)	300	
silver (Ag)	600	
rhodium (Rh)	600-900	800

to switch shorting [12]. Adhesion of contacts during hot switching is attributed to microwelding due to local heating at the metal contact surface [13].

There exist studies aiming to prevent the contact failures seen in MEMS switches, such as the work of Patton et al. In their work, they applied a self-assembled monolayer (SAM) lubricant to MEMS switch surface. At low current, lubricated contacts failed due to increase in both adhesion and contact resistance at about 10^5 cycles. Moreover, at high current, switch contacts failed immediately due to SAM thermal decomposition [14]. In another work of the same group, bimetallic nanoparticles (NPs) were used as lubricant instead of SAMs. NPs consisted of $\sim$ 2-3 nm diameter Pd NPs coated over $\sim$ 10 nm diameter Au NPs as cores. Experiments showed durability at high current with no failure through 10^6 hot switching cycles [15]. Despite these efforts, adhesion, high contact resistance, and contact bouncing continue to be problems yet to be solved for MEMS devices.

1.2 Motivation of the Work

When compared to MEMS counterparts, solid-state semiconductor switches are faster with nanosecond versus microsecond switching times [5]. Due to the absence of solid-solid mechanical contact they have no problems related to contact bounce or contact degradation. Therefore, they have very long operational lives. However, they have a high ON-state resistance of 2-6 Ω, low open-state impedance on the order of 10^5-10^7 Ω, and low power-handling capabilities [5]. Also, their sensitivity to temperature and radiation limits their range of operating environments. In addition, MEMS switches exhibit almost zero electrical power dissipation when compared with the high-current and power dissipating solid-state counterparts.

The main motivation behind our efforts in using liquid-solid MEMS (LS-MEMS) switches with liquid metal droplet actuation for electrical switching lies in the inherent advantages compared to solid-state switches and conventional solid-solid contact MEMS switches. When compared to solid-state switches, microelectromechanical liquid metal-droplet based switches provide higher isolation and lower insertion loss [16]. In addition, since they do not have fragile moving parts, LS-MEMS devices potentially do not suffer from the fatigue problems, increased contact resistance, and stiction/adhesion. They have the potential of being reliable devices without significant degradation during the lifetime of the switch.

1.3 Objectives

In this work, we have fabricated microfluidic-MEMS hybrid platforms and investigated the actuation of metallic liquid droplets, namely EGaIn, Galinstan, and Hg using EWOD. EGaIn and Galinstan were used because these materials are known as non-toxic room-temperature liquids [17]. We have investigated the effect of different actuation electrode geometries like rectangular, interdigitated fingers, and crescent-shaped electrodes on the droplet actuation. Additionally, the effect of dielectric material and its thickness on the actuation voltage, and repeatability were investigated.

1.4 Organization of the Thesis

This part of the chapter gives information about the progression of the thesis. Chapter 2 gives a theoretical background and review of operation principles of devices utilizing EWOD principle, and then it continues with explaining the effect of various device design parameters on the metallic droplet actuation. Chapter 2 ends by covering information on the liquid metal droplets used in this work and liquid-metal based EWOD devices literature review. Chapter 3 explains fabrication principles of our LS-MEMS device structures, and then details the techniques and equipment used in characterization of materials and devices fabricated in this work. Chapter 4 discusses the material and device characterizations, and analysis of fabricated LS-MEMS devices. Finally, Chapter 5 concludes the thesis with a summary, final remarks, and future work suggestions.

Chapter 2

Theoretical Background and Literature Review

2.1 Device Physics

To understand the basic mechanism of electrowetting effect, one can consider the interface between a metal electrode and an electrolytic fluid, as shown in Figure 2.1(a). When an external electric potential is applied between the metal electrode and the electrolytic fluid, the charges and dipoles redistribute, and a layer of charge builds up on the surface of the metal electrode. Repulsion between like charges in the liquid leads to a decrease in the work done in expanding the surface area, i.e., the surface tension of the liquid droplet decreases. As a result, the droplet spreads over the metal electrode area (Figure 2.1(b)). This phenomenon is called electrowetting.

Although the diffusion of charges in the liquid occurs over distances typically on the order of a few angstroms, the change in potential is not observed instantaneously. Helmholtz proposed a model for the layer consisting of these charges as a parallel plate capacitor, called "electric double layer" (EDL), where the metal surface is one plate, and an imaginary layer of charge in the liquid is the other plate (Figure 2.2) [18]. The distance between the plates would equal the

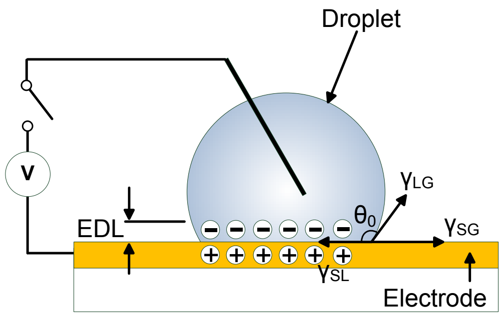

(a) (b)

Figure 2.1: Schematic representation of electrowetting effect: (a) No voltage applied. Charges are distributed at the electrode-electrolyte interface and build an electric double layer (EDL). (b) When voltage is applied, charge density at EDL changes so that surface tension between the solid and the liquid (γ_{SL}) and the contact angle change.

approximate width of the diffuse interphase region in the liquid, over which the electric field drops to near zero. Thickness of EDL varies on the order of 10-100 Å depending on the kind of electrolyte-metal pair, concentration of the electrolyte, and temperature [19].

Assuming that the width of EDL is small compared to the curvature of the surface, its capacitance per unit area can be calculated by [18]:

$$C/A = \frac{\epsilon_r \epsilon_0}{\delta}, \tag{2.1}$$

where ϵ_0 is the permittivity of free space, ϵ_r is the relative permittivity of the electrolyte, and δ is the thickness of the double layer. Since δ might be quite small, the capacitance of EDL might reach values on the order of 10 μF/cm^2 [18].

The relationship between the applied voltage and the surface tension can be derived by doing a thermodynamic analysis of the interface, and it can be expressed by Lippmann's equation as follows:

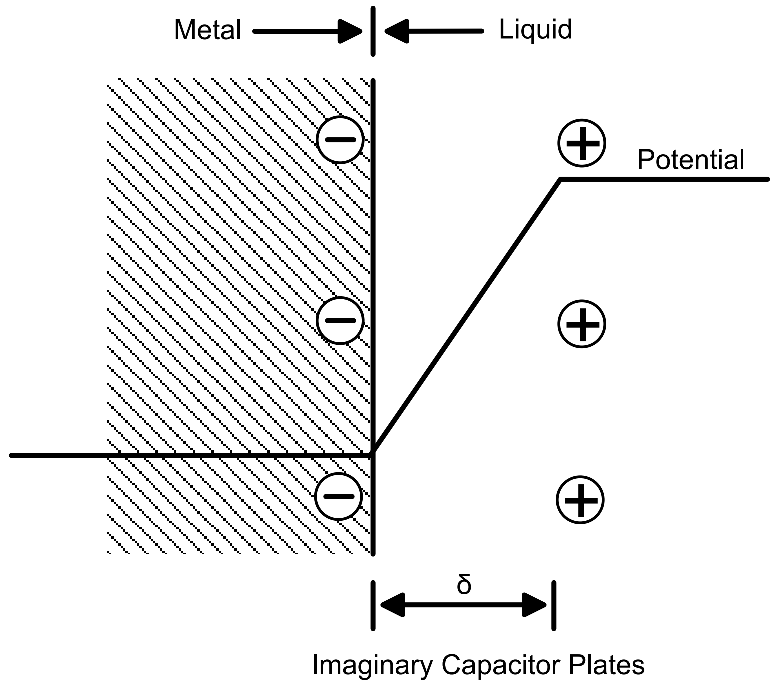

Figure 2.2: Helmholtz model of the electric double layer (EDL). Although the charge distribution in the liquid actually diffuses, it is modeled as a sheet of charge a distance δ from the metal surface.

$$\gamma = \gamma_0 - \frac{1}{2}cV^2, \tag{2.2}$$

where γ is the final surface tension, V is the applied voltage, γ_0 is the surface tension of the solid-liquid interface at the potential zero charge, and c is the capacitance of EDL per unit area [20].

Electrowetting works only with combinations of metal electrode and electrolytes that can generate a polarizable interface. Moreover, because only a small voltage drop can be sustained across the EDL, the contact angle change ($\Delta\theta$) that can be induced by conventional electrowetting without the electrolysis of the liquid is relatively small, limited by electron transfer from the electrode to redox-active species in the liquid [7], [20].

The effect of the EDL can be enhanced by coating a dielectric layer between the electrode and the liquid. The resulting phenomenon is called "electrowetting on dielectric" (EWOD) (Figure 2.3). The dielectric prevents electron transfer, while sustaining the high electric field at the interface resulting in charge redistribution when voltage is applied. Besides, irrespective of the polarization of the interface, any kind of liquid can be used in EWOD [20]. Figure 2.4 shows successful reversible actuation of a water droplet on a sample EWOD device.

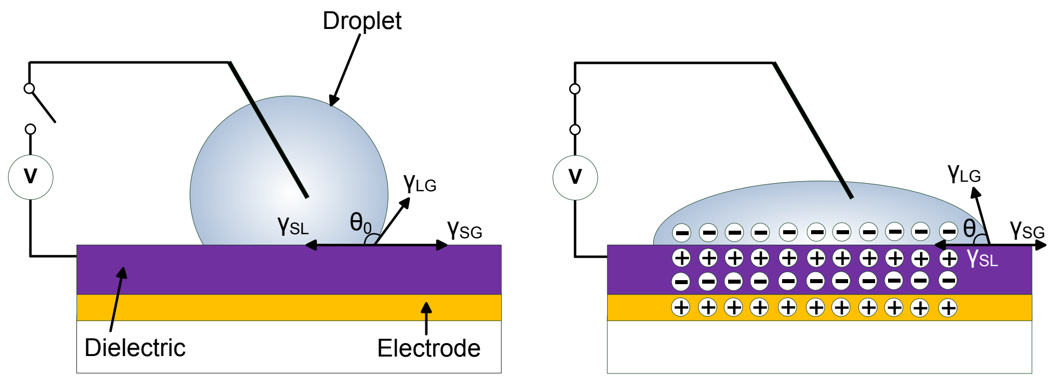

(a) (b)

Figure 2.3: Principle of EWOD. (a) With no voltage applied, there is little or no charge accumulation at the interface. (b) When voltage is applied, charge accumulates at the interfaces. γ_{SL} and the contact angle decrease.

In the case of EWOD, Lippmann's equation (Eq. 2.2) can be expressed in terms of the contact angle θ by incorporating Young's equation (Eq. 2.3). The resulting equation (Eq.2.4) is called the Lippmann-Young equation.

$$\gamma_{SL} = \gamma_{SG} - \gamma_{LG}\cos\theta, \tag{2.3}$$

$$\cos\theta = \cos\theta_0 + \frac{1}{\gamma_{LG}}\frac{1}{2}cV^2, \tag{2.4}$$

where θ_0 is the contact angle when no voltage is applied, γ_{SL} is the solid-liquid surface tension, γ_{LG} is the liquid-gas surface tension, and γ_{SG} is the solid-gas surface tension. Here, γ_{LG} and γ_{SG} are assumed to be constant, independent of the applied potential [20].

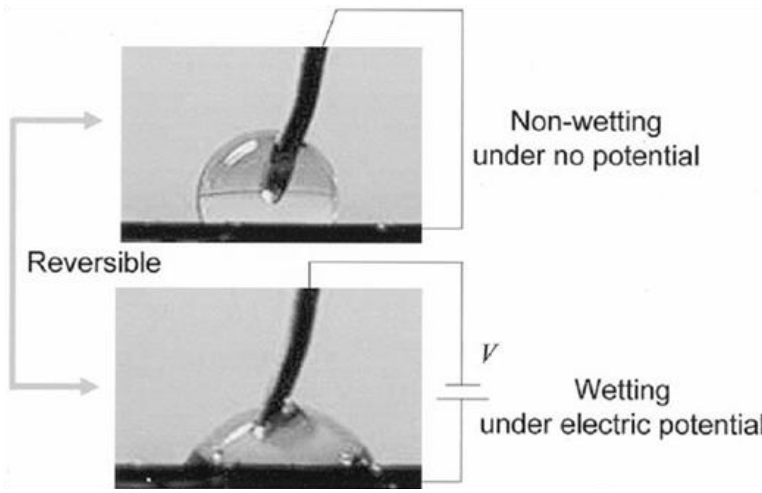

Figure 2.4: Reversible actuation of a water droplet on a sample EWOD device [21].

The electrowetting equation is verified experimentally for aqueous conductive liquids, and the smallest contact angle reported was 30°. The surface tensions of liquid metals, such as mercury and gallium-indium-tin alloy (which are liquid at room temperature), are much larger than that of aqueous liquids, which implies that a higher voltage is needed to achieve the same contact angle change [22].

Eq. 2.4 suggests that the contact angle (θ) is a function of the applied voltage. Moreover, as stated in [20], a significant contact angle change (for example from 120° to 80°) is desired to actuate and move the droplet. Unless it leads to unintentional actuation due to superhydrophobicity of the surface, the higher the initial contact angle, the better and easier the actuation is. The required voltage to induce a specified $\Delta\theta$ is proportional to the square root of the thickness of the dielectric layer with a fixed dielectric constant (Figure 2.5). In addition, the breakdown voltage of the dielectric layer is proportional to the thickness. As shown in Figure 2.5, below a certain thickness, the dielectric layer might be possibly damaged before the desired contact angle change is obtained [20].

The specific capacitance of a dielectric layer is:

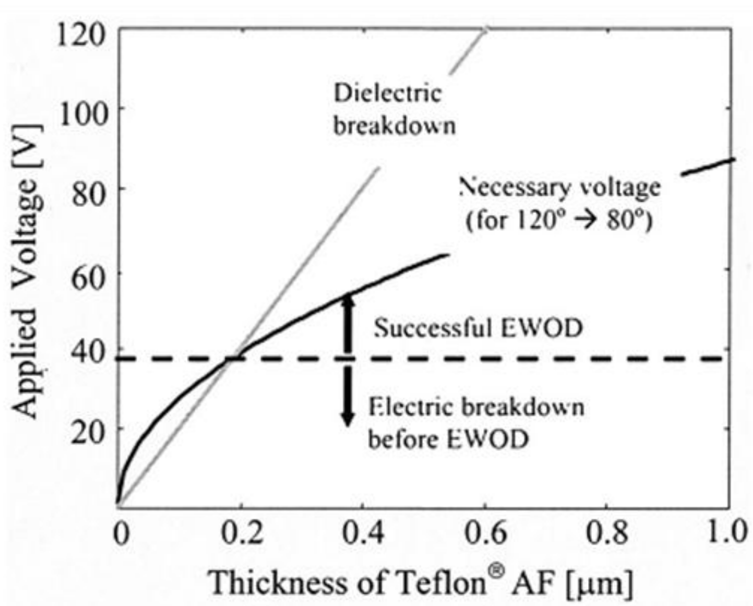

Figure 2.5: Applied potential needed to achieve a specified contact angle change ($\Delta\theta$) by EWOD, and breakdown voltage for the same dielectric layer as function of thickness. The dielectric layer is assumed to be Teflon AF, with ϵ=2.0 and $E_{breakdown} = 2 \times 10^6$ V/cm [20].

$$c = \epsilon_0 \epsilon / t, \tag{2.5}$$

where ϵ_0 is permittivity of vacuum, ϵ is the dielectric constant of the dielectric material, and t is the thickness of the dielectric layer.

In order to actuate a droplet in an EWOD device, an electric field is applied to the electrode next to it while others are grounded. This electric field induces negative charges on one side of the droplet surface closest to the electrode and positive charges on the other side (Figure 2.6). The induced charges create the Maxwell stress through the electrostatic force [23].

On the other hand, there are two resistive forces to the movement of the droplet. The dominant resistive force is the contact angle hysteresis (CAH) force stemming from the small size of the droplet (100-1000 μm depending on the design) [9]. It is due to the surface tension of the liquid droplet and defined by the difference

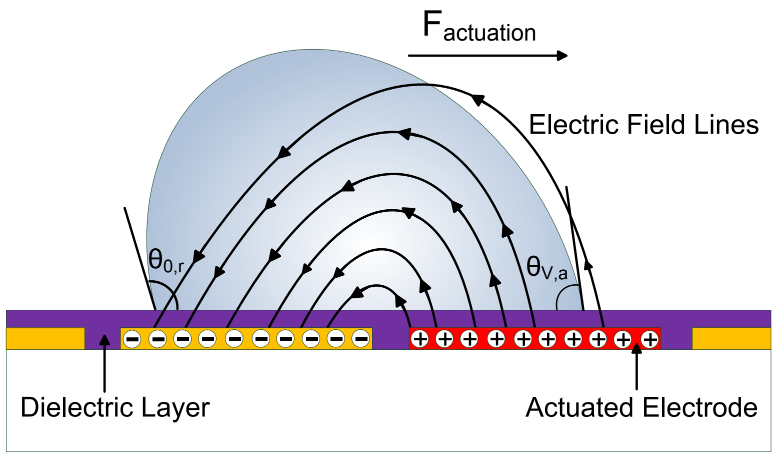

Figure 2.6: Electric field distribution in an EWOD device during actuation.

between the advancing and receding contact angles (Figure 2.7(a)), which can be measured by the classic tilting-plate method. Another critical aspect of the electrowetting is surface hysteresis, which is ignored in the electrowetting equation, but needs to be seriously considered. Low-hysteresis surface is a requirement for large and reversible electrowetting actuation. The maximum contact angle hysteresis force occurs when the difference between the two contact angles become maximum. The maximum (minimum) contact angle is called the advancing (receding) angle. For this purpose, a hydrophobic layer such as Teflon can be coated on top of the dielectric layer [22]. The electrowetted advancing angle ($\theta_{V,a}$) is smaller than the inherent receding angle ($\theta_{0,r}$) (Figure 2.7(b)) [8], [9]. If the static force is large enough to overcome the surface tension of the droplet, the droplet moves onto the electrode upon the voltage is applied [23].

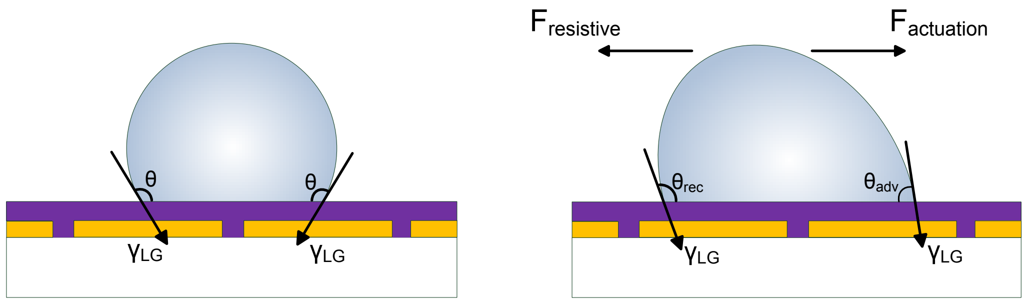

Figure 2.7: Forces acting on a liquid droplet during actuation.

2.2 Device Design Parameters

Every type of EWOD device structure comes with its unique design requirements. For example, for a LoC device, it is necessary to move the fluidic sample or droplet to be analyzed into the microchannels. For this purpose, to achieve actuation at a reasonable voltage level, the electrode spacing and channel gap should be fine-tuned. In a liquid-metal EWOD switch for potential RF applications on the other hand, parameters of the transmitted signal such as latency, isolation, and insertion loss are important. In order to meet these requirements, different device designs have been proposed by different research groups as explained in Section 2.3.3 below.

For any kind of electrical switch, high switching speed, i.e., low latency, is a desirable property. An EWOD switch utilizing a droplet as the active switching element can meet this requirement only by having a small switching gap. This means that the droplet has to travel a very short distance when actuated. The design used in this work, therefore has a switching gap around 10 μm (Figure 2.8).

Grounding of the actuated droplet is another design consideration. Electrowetting force is lower in devices with no droplet grounding compared with that of the ground-type electrowetting devices. This lower force is attributed to the fact that only a portion of the applied voltage contributes to the electrowetting force generation. What happens is that the applied voltage drops across two dielectric

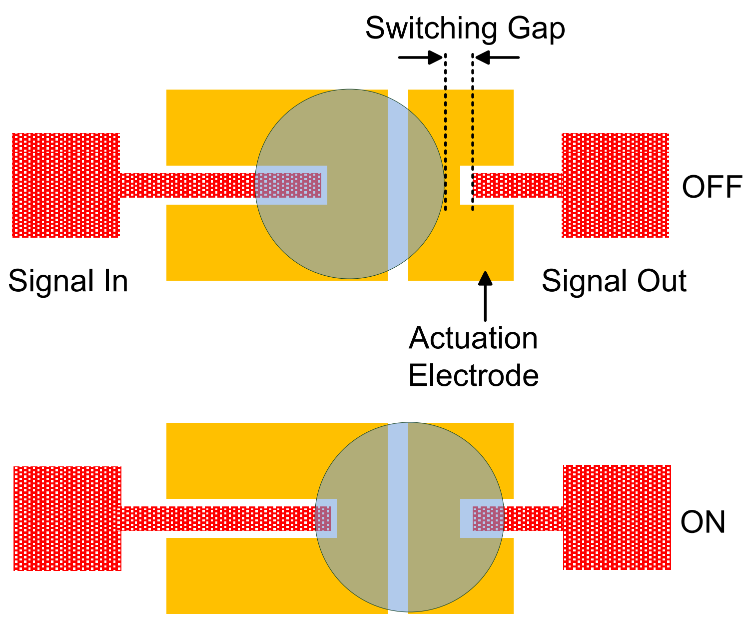

Figure 2.8: Schematic showing the switching mechanism and the switching gap in an EWOD switch.

layers: one part is between the activated electrode and the droplet, and the other part is between the reference electrode and the droplet. Since the force applied in electrowetting is proportional to the square of the applied voltage across the dielectric layer, the effective net force is further reduced when the voltage drop across the dielectric layer decreases [8]. Taking this fact under consideration, devices in this work were fabricated by etching the dielectric layer on top of the reference electrode. This was done during the fabrication step in which the oxide layer on top of the contact pads were etched.

Successful droplet actuation using EWOD also requires the droplet to have a high initial contact angle. This way the contact angle change, i.e., the actuation force applied on the droplet, can be increased. For this purpose, a hydrophobic layer (in our work, Teflon AF2400) is coated on top of the dielectric layer, which provides room for a large contact angle change upon electrowetting.

Another design criterion for an EWOD device is the capacitance [1]. Since the energy stored in the capacitor determines the force applied to the droplet

[1], it is advantageous to increase the capacitance. This can be achieved in two ways: either by decreasing the dielectric layer thickness or by using a dielectric layer having a higher dielectric constant. The use of a high-k dielectric may easily reduce the voltage required to actuate a droplet. Decrease in thickness, on the other hand, may cause an early breakdown of the dielectric before successful droplet actuation. Moreover, it is generally observed that as the dielectric becomes thinner, the contact angle saturates early (i.e., at a large angle). Moon et al. report that in their work, the contact angle saturated at $\sim 60°$ on the 12 mm Parylene sample, $\sim 75°$ on the 1 mm oxide sample, and $\sim 80°$ on the 100 nm oxide sample (Figure 2.9). There are different studies trying to explain the reason of early contact angle saturation. While Peykov et al. stated that contact angle saturates when the surface energy of solid-liquid interface becomes zero [20], Vallet et al. suggested that it happens at the voltage corresponding to the onset of air ionization. In another work, it was speculated that trapped charges in the dielectric layer play a role in saturation [24]. In the work of Seyrat et at., contact angle saturation was reported to be a material deficiency. Therefore, a balance should be sought between the dielectric layer thickness and dielectric constant [20].

Since LS-MEMS switches in this work utilize SU-8 microframe for droplet positioning, it is important to consider its effect on the position of contact line. Figure 2.10 shows the schematic top view (left) and side view (right) of the microframe structure. For the sake of simplicity, all curved sections are assumed to be circular during calculations. The radius of curvature of the positioned liquid metal droplet at the larger opening of the microframe can be expressed as:

$$R = \frac{h}{2\cos\theta_\omega}, \tag{2.6}$$

where R is the radius of curvature of the positioned liquid metal droplet at the larger opening, h is the width of the larger opening, θ_ω is the contact angle between the liquid metal droplet and the SU-8 sidewall.

The device is enclosed from above by the glass top plate, as can be seen from

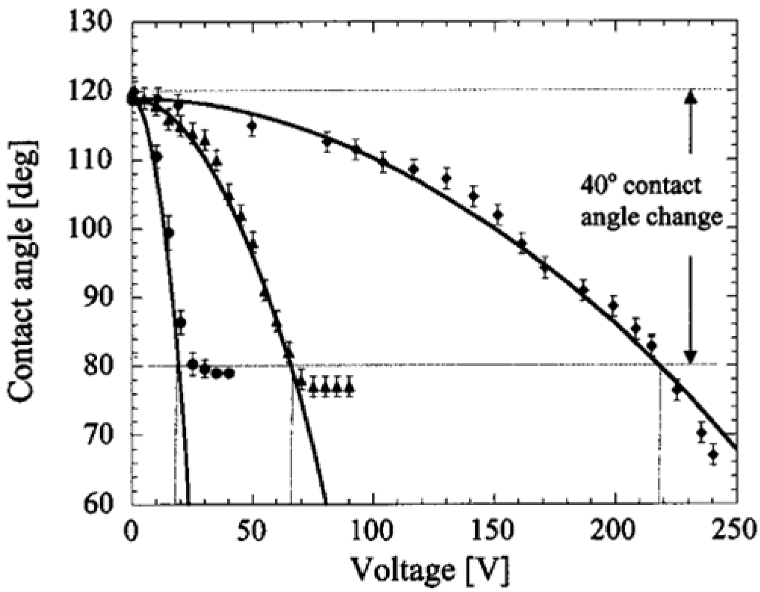

Figure 2.9: Contact angle change with applied voltage for three dielectrics, showing the effect of thickness. Solid lines are based on Eq. 2.3 and solid markers denote experimental results. From the left: 100 nm oxide (circles), 1 μm oxide (triangles), and 12 μm Parylene (diamonds). All dielectric insulation layers were coated by 200-Å-thick amorphous fluoropolymer [20].

the side view in Figure 2.10. The other radius of the curvature, which is due to the top plate, can be expressed as:

$$r = \frac{g}{2\cos\theta_s}, \tag{2.7}$$

where r is the radius of the curvature which is due to the top plate, g is the top plate gap, and θ_s is the contact angle between the liquid metal droplet and the top plate. The Laplace pressure is the pressure difference between the inside and the outside of a liquid droplet. The effect is caused by the surface tension of the interface between liquid and gas, and can be expressed as:

$$\Delta P \equiv P_{inside} - P_{outside} = \gamma\left(\frac{1}{R_1} + \frac{1}{R_2}\right), \tag{2.8}$$

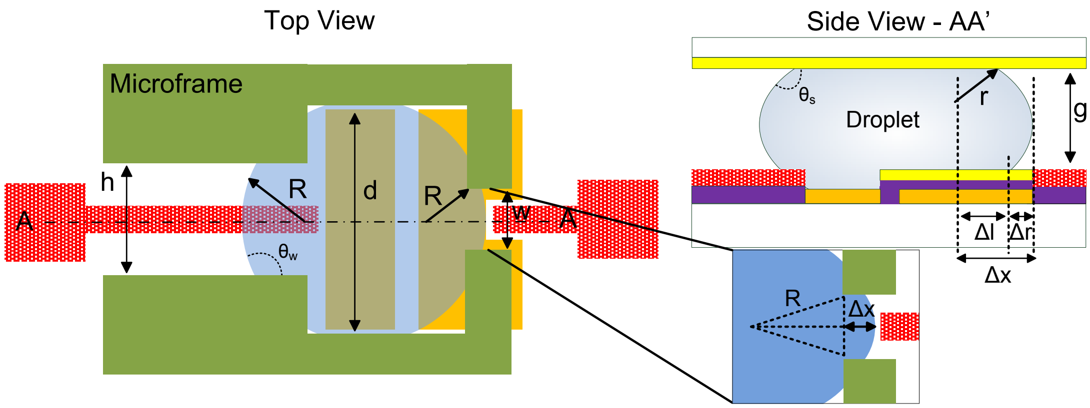

Figure 2.10: Schematic drawing of a sample device with SU-8 microframe. In the top view, the larger left opening and the smaller right opening are shown.

where R_1 and R_2 are the radii of curvature, and γ is the surface tension of the droplet. The Laplace pressure of the droplet in this work can be calculated by:

$$\Delta P = 2\gamma \left(\frac{\cos\theta_\omega}{h} + \frac{\cos\theta_s}{g} \right), \tag{2.9}$$

If it is assumed that $\theta_\omega \approx \theta_s$, the Laplace pressure is determined by the two openings, i.e., h and g. Since it requires higher pressure for the droplet to deform along the smaller opening, it is more favorable for it to deform its interface along the larger dimension. Moreover, in the device design, the magnitude of the larger opening and the plate gap are equal in order to ease the interface deformation when absorbing the droplet-volume variation [6].

Due to the fact that the pressure is constant inside the droplet, the radius of curvature at the larger (left) opening is equal to that at the smaller (right) opening. Although a larger right opening is desirable for the sake of larger overlaps with actuation electrode, and thus in a lower actuation voltage, it results in a higher uncertainty in the contact line position. Therefore, the small opening ω is restricted by the rule $\omega < h$. To calculate the contact-line position at the right opening, Δx and Δr, shown in side view in Figure 2.10, should be calculated [6]. From Figure 2.10, Δx is calculated as:

$$\Delta x = R - \sqrt{R^2 - \left(\frac{\omega}{2}\right)^2}, \tag{2.10}$$

where R is calculated from Eq. 2.6, and Δr is calculated from the side view in Figure 2.10 as:

$$\Delta r = \frac{g\left(\sin\theta_s - 1\right)}{2\cos\theta_s}, \tag{2.11}$$

Finally, at the right opening, the position of the contact line from the inner edge of the microframe is obtained as:

$$\Delta l = \Delta x - \Delta r, \tag{2.12}$$

2.3 Liquid Metals and Literature Review for Liquid Metal-based Switching Devices

2.3.1 Mercury

Mercury is a low-viscosity, Newtonian fluid (like water or oil), and does not oxidize readily (i.e., does not form a skin) under ambient conditions [17]. Having a melting point of -38.83°C and a boiling point of 356.73°C, it is the only metal that is liquid at standard conditions for temperature and pressure. Mercury is used in thermometers, barometers, manometers, float valves. Although its resistivity is higher compared to gold, $9.61\text{x}10^{-5}\Omega\cdot\text{cm}$ at 25°C versus $2.21\text{x}10^{-6}\Omega\cdot\text{cm}$ at 20°C, mercury can be used as active switching element in electrical switches with high performance. Even at very high frequencies (15 GHz), mercury has been reported to show very low insertion loss, which is comparable to copper through-connects [25].

Mercury brings advantages as a result of its inherent properties. For example, due to high surface tension (435 mN/m) mercury droplets act like a solid ball. Moreover, because of its low adhesion to metallic and dielectric surfaces, no residue is found when mercury is moved from one location to another, making it an ideal liquid metal [26]. However, due to its toxicity, the use of mercury has been limited stemming from concerns about environmental hazards and health issues [5].

Since mercury is a metal rather than an electrolyte, there will be no double layer upon the application of a voltage; instead, a substantial current will flow [18]. Thus, in order to create a capacitance and actuate a mercury droplet, a dielectric layer must be coated on top of the actuation electrodes.

One of the preferred deposition methods for mercury is based on selective condensation of mercury vapor on gold dots acting as preferred nucleation sites. This method allows the control of droplet dimensions and locations, and is suitable for batch fabrication [27]. However, the maximum droplet diameter is reported to be limited to 30 μm due to random nucleation. Although there are no published data on the deposition accuracy, achieving better than 1 μm accuracy for a 30 μm droplet is considered difficult in practice [6].

Another possible technique for mercury droplet deposition is a commercial liquid jetting system JetLab from MicroFab Inc., which jets small droplets with diameter depending on the jetting nozzle diameter and the jetting voltage waveform [28]. In their work, Sen et al. were able to achieve 30 μm droplets from a 60 μm jetting nozzle diameter. Moreover, by carrying out multiple depositions at the same location, larger diameter ($\sim$ 100 μm) droplets were achieved with less than 3% variation in the diameter [6].

2.3.2 EGaIn and Galinstan Liquid Metals

Eutectic Gallium-Indium (EGaIn) is an electrically conductive fluid metal alloy, consisting of 75 wt.% Ga and 25 wt.% In. While its melting point is 15.5°C, its boiling point is undetermined yet. The surface tension of EGaIn at ambient conditions is 624 mN/m [17], whereas the surface tension of EGaIn during exposure to aqueous HCl, which is thought to cause acid-promoted dissolution of the oxide at the surface, is 435 mN/m. Experiments conducted in microfluidic channels and in a parallel-plate rheometer suggest that EGaIn's behavior is mainly defined by the properties of its surface (predominantly gallium oxide - an n-type semiconductor [29]- as determined by Auger measurements); these two experiments both yield approximately the same number for the critical surface stress required to induce EGaIn to flow (0.5 N/m).

The resistivity of EGaIn is $\sim 29.4\text{x}10^{-6}\text{V}\Omega \cdot \text{cm}$; this property allows EGaIn to be used as a contact electrode for the electrical characterization of thin-film organic and semiconductor devices.

The work of Chen et al. demonstrates a non-toxic liquid metal shunt capacitive switch, which is based on a liquid metal slug flowing in the channel above a co-planar waveguide (CPW) line (Figure 2.11). Designed for very wide-band application from 2 to 100 GHz, the switch utilizes a Teflon solution from DuPont, Teflon AF 400S1-100-1, 1% Teflon powdered resin dissolved in 3M FC-75. In order to move the solution in and out the 500-μm wide microchannel, Teflon tubes with inner diameter of 500μm are employed as the external tubes. Since it forms an immiscible solution with the Teflon solution, Galinstan does not stick to the channel. When Galinstan overlaps the CPW line it does not directly contact the line because of this thin Teflon layer. As a result, it behaves like a shunt capacitor which shorts the RF signal. The test device achieves an ON-state shunt capacitance of 4 pF with a 60/100/60-μm CPW line. The ON-state insertion loss of the switch is nearly equal to the loss of the transmission line [26].

Galinstan, which is also liquid at room temperature with melting point at -19°C, is an eutectic alloy of 68.5% Ga, 21.5% In, and 10% Sn by weight. The boiling point of Galinstan, 1300°C, is higher than mercury's, 356.73°C, which makes Galinstan a good candidate for high power and temperature applications. Due to its non-toxicity, it is currently being used to replace mercury in thermometers [26].

Severely fast oxidation of Galinstan and EGaIn in air poses a great difficulty in handling them, which becomes especially significant in microscale because of

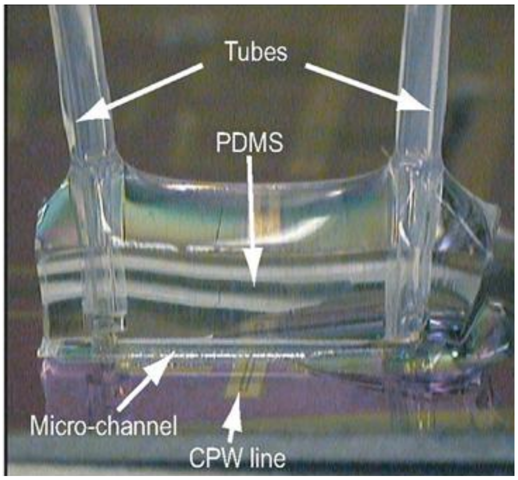

(a)

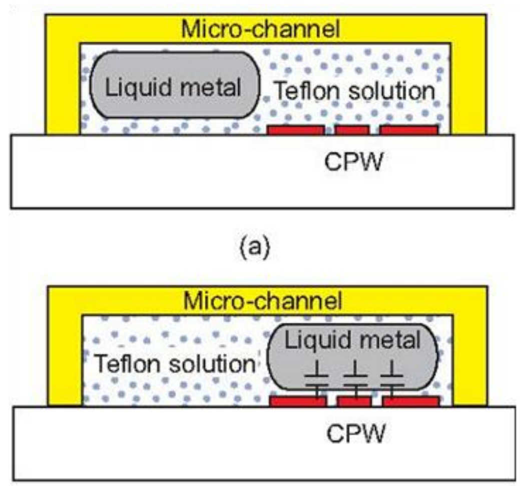

(b)

Figure 2.11: Microfluidic switch using Galinstan slug. (a) Complete structure. (b) Schematic representation of the working principle of the switch [26].

the large area-to-volume ratio, so that droplets might form a distinctively non-spherical shape, even at only 0.2% oxygen in a nitrogen-filled glove box. However, as shown in Table 2.1, Galinstan droplets show no apparent effect of oxidation when the oxygen amount reduces $\sim$ 0.1 ppm. Therefore, although Galinstan is usually assumed to wet almost all surfaces, it is the oxidation of Galinstan that produces the appearance of wetting [30].

Table 2.1: Behavior of Galinstan droplet at different oxygen trace levels [30]

Oxygen	**Observation**
0.2-20.9%	Droplet is distinctively non-spherical by instantaneous surface oxidation even at the moment of dispensing.
$\sim$ 20 ppm	Droplet is spherical. Droplet behaves like gel rather than true liquid.
$<$ 1 ppm	Droplet behaves like true liquid.
$<$ 0.5 ppm	Droplet behaves like true liquid.

In the work of Liu et al., in a glove box, advancing/receding contact angles of Galinstan on a glass and Teflon surface are 146.8°/121.5° and 161.2°/144.4°, respectively. On a $\sim$ 170 nm-thick Teflon AF surface, contact angle is measured to be 151° and decreased to $\sim$ 113° when the voltage increased to 120 V [30].

Table 2.2 shows the compatibility of gallium with metals used in MEMS. Depending on the device design, the list of candidate materials is quite limited. However, chromium, copper, and tungsten can be used unless temperatures as high as 600°C are reached.

Table 2.2: Compatibility of Gallium with metals used in MEMS [5]

Elements	**Reactivity**
Aluminum	Readily attacks
Chromium	Reacts readily at temperatures $>$ 600°C
Copper	Fuses into and attacks at high temperature
Germanium	Forms a semiconducting compound
Gold	Solubility increases with temperature
Indium	Dissolves with unlimited miscibility
Nickel	Reacts readily
Platinum	Readily attacks
Silicon	Dissolves
Silver	Forms compounds
Tantalum	Resistant but corrodes when exposed to air
Titanium	Disintegrates at 450°C forming Ga_3Ti
Tungsten	Slight attacks only at temperatures $>$ 800°C

An example of a device utilizing Galinstan is demonstrated in the work of Mazlouman et al. It is a reconfigurable patch antenna which uses Galinstan by embedding it in a TC5005 silicone substrate [31]. The presented design can be stretched by up to 300% and the antenna can operate at a frequency located from 1.3 to 3 GHz.

2.3.3 Liquid Metal-based Switches

This part of the chapter discusses advances in the EWOD-based technology summarizing the best-reported results for liquid metal droplet-based switches.

Liquid metal droplets have been actuated by i) electrothermal [32], [33], ii) electrostatic [3], [34], and iii) EWOD [28], [35] methods to achieve switching operation. However, there is contradictory information about who actually made the first use of the electrowetting effect. In [24], it is stated that Minnema made use of it in 1980 by coating a dielectric layer between the liquid and the metal electrode [36], and he was followed in 1981 by Beni, who used a liquid directly on the metal electrode [37]. On the other hand, [38] states that Washizu first reported on electrostatic actuation of liquid droplets on the unground-type single-plate device in 1998.

An example of liquid metal switches actuated by EWOD method is the one reported by Sen et al. In their work, mercury droplets are positioned between two substrates and are actuated by a fringe field based capacitive drive. Electrowetting experiments showed significant variation from theory due to dielectric charging. However, by the application of positive bias to the droplet, the charging effects reduced and gave results in good agreement with the theory. They report devices with actuation voltages of 80 V and actuation speed of more than 3.3 cm/s [35].

Another device which Sen et al. demonstrated is a liquid metal droplet based MEMS switch with 60 μs switch-on latency, which they report to be around 20 times better than other liquid metal switch technologies. The reason for the better latency, they state, is the design of microswitches with very small switching gaps, for example 10 μm for 600 μm-diameter droplets. Moreover, in this work, by positioning the droplet inside a microframe structure, only the contact line is actuated instead of moving whole droplet. The authors report contact resistance of 2.35 Ω for a 50 μm x 50 μm Ni-Hg contact and switch-off latency of 150 μs [39].

Chen et al. report an electrostatic liquid-metal capacitive shunt MEMS switch, where a mercury droplet with a diameter of 1 mm capacitively loads a CPW line. Since the droplet has the ability to successfully conform over the 50/80/50 μm CPW line, the switch achieved a large shunt capacitance of 4 pF. Actuation voltage of the droplet was measured to be 110 V. Moreover, the switch is reported to demonstrate an off-state loss of less than 0.6 dB up to 20 GHz, which is only due to the transmission line. The switch isolation is 15.7 dB and 21.1 dB at 10 and 20 GHz, respectively [9].

Chapter 3

Experimental Details

In this chapter, first, the LS-MEMS device fabrication process including the detailed step by step microfabrication processes, process equipment details, and the process parameters (recipes) are described. Afterwards, the equipments used in characterization experiments are introduced. Finally, characterization techniques for the LS-MEMS devices fabricated and droplet actuation experimental setup are introduced.

3.1 Device Fabrication

This part details the five-mask-level processing steps that are performed for the fabrication of the liquid metal switch, all of which were conducted in class 100 and class 1000 facilities at UNAM Cleanroom Facility (UCF) at Bilkent University. Fabrication is performed on 4'' fused silica or quartz wafers. Photomasks used during photolithography were designed using L-Edit software from Tanner Tools. The mask writing was performed with a Heidelberg Instruments DWL-66 Laser Mask Writer in UCF (Figure 3.1).

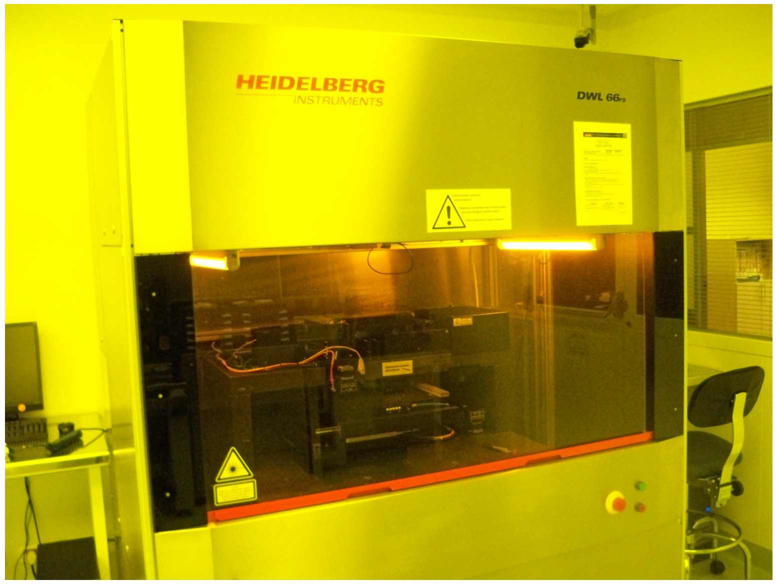

Figure 3.1: Heidelberg Instruments DWL-66 Laser Mask Writer used for writing the photomasks.

3.1.1 Substrate and Surface Preparation

Surface preparation and cleaning before device fabrication is critical for the performance of the devices and repeatability of the processes. Cleanliness of the wafers is crucial since any dirt may prevent the devices from working properly. Thus, samples were first ultrasonically degreased in a 5-min acetone ($(CH_3)_2CO$) bath, followed by a 5-min isopropyl alcohol ($(CH_3)_2CHOH$) bath (Figure 3.2(a)). They were then rinsed thoroughly in deionized (DI) water and dried by a nitrogen gun. Finally, the wafers were dehydration-baked on a controlled hot-plate at 120°C for 5 min, in order to eliminate any possible H_2O contamination on the wafer surface (Figure 3.2(b)). This cleaning procedure was repeated after each completion of a process step and prior to the start of a new photolithography or deposition process.

(a) (b)

Figure 3.2: (a) Samples were first ultrasonically degreased in a 5-min acetone ($(CH_3)_2CO$) bath, followed by a 5-min isopropyl alcohol ($(CH_3)_2CHOH$) bath. (b) They were dehydration-baked on a controlled hot-plate at 120°C for 5 min.

3.1.2 Metallization and Patterning of Actuation Electrodes

As the next step of the fabrication process, a 100-nm-thick chromium (Cr) layer was sputtered using VAKSIS Sputter system (Figure 3.3). Samples were rotated during sputtering to enable conformal sidewall coverage and also uniform deposition rate on sample surface. The coating parameters used were: 150 W plasma power, 8 mTorr chamber pressure and 70 sccm Ar flow rate. The measured deposition rate using these parameters was $\sim$ 10 nm/min. Coating process was not started until the chamber pressure reached at least 6×10^{-6} Torr to ensure a particle-free ambient in the reactor chamber.

After metallization, photolithography process was carried out in the UCF yellow room to transfer the desired patterns onto the substrate. First, surface dehydration of the wafer was performed on a hot plate at 120°C for 5 minutes. This step removes humidity off the surface, ensuring better photoresist adhesion and coverage as well as improving the resolution of the features. The first mask was used to define actuation electrodes and their contact pads. AZ5214E photoresist (PR) of AZ Electronic Materials was spin-coated at 4000 RPM for 40

Figure 3.3: VAKSIS Sputter system used for metallic coating processes in this work.

seconds with acceleration of 2000 RPM resulting in a 1.4-μm-thick photoresist layer (Figure 3.4(a)). Pre-exposure bake was carried out on a hot plate at 110°C for 50 seconds to remove solvents in the photoresist. Electronic Vision Group EVG620 Mask Aligner was used for i-line UV (λ = 365 nm) exposure of the spin-coated photoresist layer using constant dose of 75 mJ (Figure 3.4(b)). The exposed patterns were developed in AZ400K developer (AZ400K:H_20 = 1:5) for 40 seconds.

After photolithography, descum process was carried out in the NanoPlas-DSB6000 Plasma Asher for 1 minute in oxygen ambient (30 sccm) under 550 W RF plasma power to remove the thin possible non-developed PR and improve the final patterning (Figure 3.4(c)). Next, the chromium layer was wet etched for 1 minute 30 seconds in Chromium Etchant of Technic using the patterned PR as etch-mask. After the chrome film was completely etched with a rate of $\sim$ 100 nm/min, the PR was removed using acetone followed by isopropyl alcohol cleaning. Finally, the patterned chrome wafer was rinsed in DI-water and dried by a nitrogen gun (Figure 3.5).

(a)

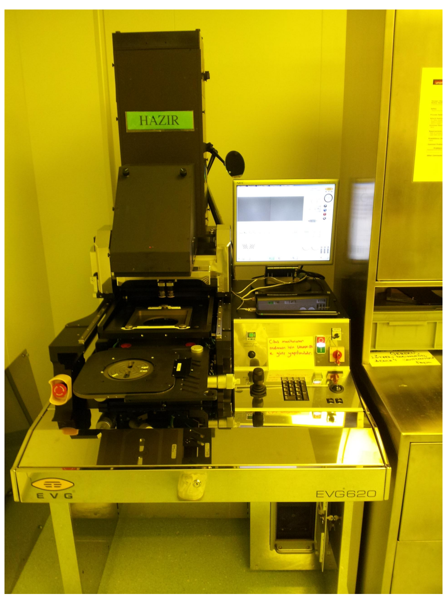

(b)

(c)

Figure 3.4: (a) Spinning of the PR on top of the wafers were done in Laurell spinner system. (b) Electronic Vision Group EVG620 Mask Aligner used for exposure of the PR coated wafers. (c) Descum process was carried out to remove the residual PR layers before metal etch and deposition processes.

Figure 3.5: Sample device with coated and patterned Cr electrode. The contact pad below is not shown.

3.1.3 Dielectric Film Coating and Patterning

In the second processing step, a 300-nm-thick SiO_2 layer was coated using VAKSIS PECVD system as the dielectric layer in the EWOD actuator device (Figure 3.6). The process parameters used were: 10 W plasma power, 1000 mTorr chamber pressure, 350°C deposition temperature, 15 sccm N_2O, 6 sccm SiH_4 and 700 sccm He gas flows.

The deposition rate of SiO_2 with this recipe was measured using J. A.Woolam V-VASE spectroscopic ellipsometer (Figure 3.7) and it was found to be about 2.8 nm/min (Figure 3.8).

Figure 3.6: VAKSIS PECVD system used for dielectric coating processes in this work.

Figure 3.7: J. A.Woolam V-VASE spectroscopic ellipsometer.

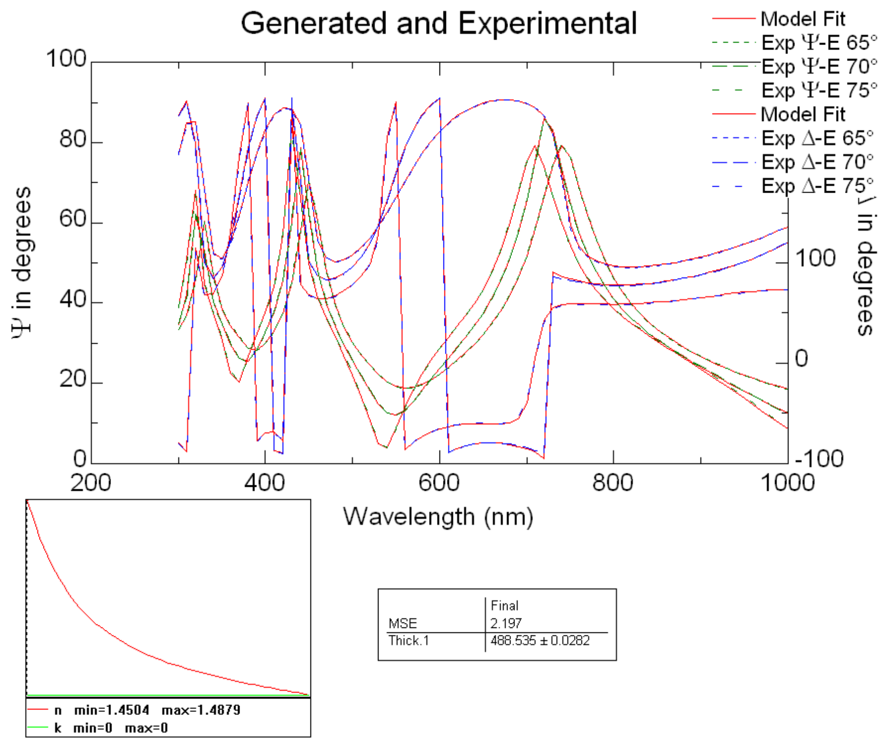

Figure 3.8: SiO_2 thickness characterization in V-VASE spectroscopic ellipsometer.

After deposition of SiO_2 dielectric layer, an image reversal (IR) photolithography process was performed to define contact windows in dielectric layer. For this purpose, after spin-coating and soft-bake, the AZ5214E photoresist was first exposed under the mask aligner with 75 mJ exposure dose, followed by an IR bake at 120°C for 1 minute 40 seconds. Next, the photoresist was exposed without mask (flood exposure), with a total additional dose of 300 mJ. The flood expose dose was higher than that would be used for Si wafers, since transparent substrates suffer from the minimal photoresist/quartz reflectivity and therefore require a higher flood exposure dose.

Development of the photoresist was carried out with ($AZ400K{:}H_20 = 1{:}4$) for 1 minute 20 seconds. The PR used for IR photolithography was AZ5214E since it can be used as a negative tone resist by baking it after first exposure and then carrying out a flood exposure.

There are two alternative methods to etch the SiO_2 layer: Either by wet etching using buffered oxide etchant (BOE) of Technic or by dry etching making use of the inductively coupled plasma (ICP) equipment. Both methods have their advantages and disadvantages. For instance, in the former, etch rate was determined to be ~100 nm/min and PR etch rate can be neglected. The advantage of having a high etch rate brings an important process design consideration: the amount of etching cannot be controlled precisely. Additionally, wet etching is an isotropic process and undercuts form as shown in Figure 3.9, since it is a purely chemical process.

Figure 3.9: Undercuts formed during wet etch of SiO_2.

On the other hand, in ICP there are two recipes with different etch rates:

i) Using CHF_3 and O_2 process gases with etch rates of 24 nm/min and 31 nm/min for PECVD SiO_2 and AZ5214 PR, respectively,

ii) Using CF_4 and O_2 process gases yielding etch rates of 52 nm/min and 176 nm/min for PECVD SiO_2 and AZ5214 PR, respectively.

Detailed process parameters for dry etching in ICP are shown in Table 3.1. In ICP PR etch rate, or etched material to PR selectivity, is an important process parameter. Therefore, among the two etch recipes mentioned, the first one was preferred during dry etch processes. Moreover, experiments with LPX SR (Cl) system of STS (Figure 3.10) revealed that it is a good practice to leave at least 200 nm-thick PR on top of the PR-protected part of the wafer at the end of etching process. This ensures high anisotropy in anisotropic processes and improved etch patterns. Lower etch rates compared to wet etching provides a more controllable etch process. This becomes advantageous especially in processes where thin layers of materials are to be etched. Finally, depending on the gases used and the processing pressure, dry etching can be isotropic or anisotropic, preventing the undercut effects seen in wet etch.

Table 3.1: Detailed process parameters for dry etching in ICP

	Recipe I	**Recipe II**
Gas 1 [sccm]	CHF_3 (100)	CF_4 (100)
Gas 2 [sccm]	O_2 (20)	O_2 (20)
13.56 MHz Coil Power [W]	250	250
380 kHz Platen Power [W]	30	30
Pressure [mTorr]	50	50
SiO_2 Etch Rate [nm/min]	24	52
PR Etch Rate [nm/min]	31	176

Figure 3.10: ICP system utilized for dry etching processes.

Among the two etching methods, dry etching in ICP using Recipe I was the preferred one due to the more controlled etching and improved etched patterns. Electrodes with deposited and patterned SiO_2 layer can be seen in Figure 3.11.

Figure 3.11: Sample device with coated and patterned SiO_2 dielectric layer.

3.1.4 Definition and Metallization of Signal Lines

The process steps for deposition of signal-in and signal-out lines of the device consist of an IR photolithography followed by sputtering and lift-off process. The patterning method of the coated Cr/Ni layer was preferred as lift-off rather than wet etch, since Ni etchant damages the Cr layer underneath during patterning. Therefore, first an IR photolithography step was performed with the third-level mask using the parameters mentioned before. Then, 100 nm/100 nm Cr/Ni layer was sputtered using VAKSIS Sputtering system. After metallization, samples were left in acetone overnight for lift-off. During lift-off, the thickness of the PR was crucial for the proper transfer of the desired patterns. The thickness of the PR should be at least twice that of the coated film. Also, the photolithography process should be optimized to form an undercut in the resist. IR photolithography parameters were optimized to obtain negative-slope side walls which leads to completely isolated deposition of metal films on the substrate and the photoresist film. A successfully lifted-off device with signal lines can be seen in Figure 3.12.

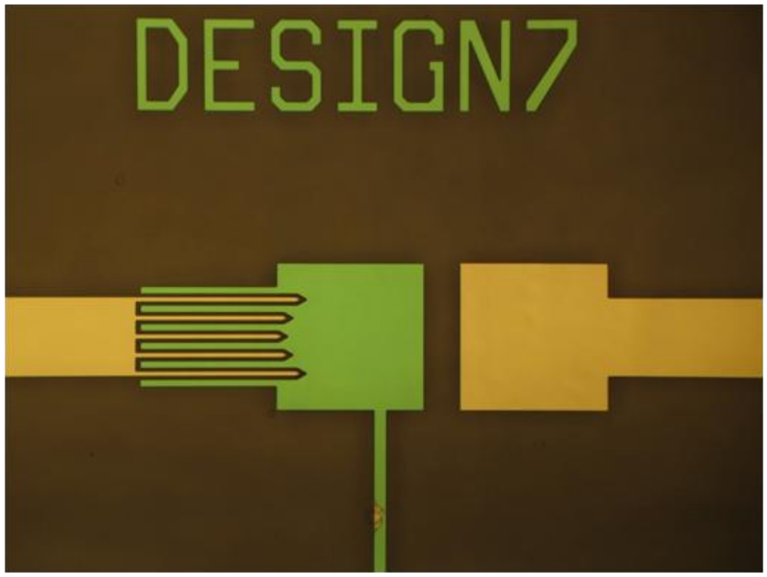

Figure 3.12: Sample device with coated and patterned Cr/Ni signal lines.

3.1.5 Coating and Patterning of Hydrophobic Layer

In microfluidic devices, contact-angle hysteresis (CAH), static friction which restricts contact line motion, causes the contact line to pin on surface heterogeneities. CAH also affects the positioning of a droplet, and the contact line, on a device. To illustrate, as reported in the work of Sen and Kim, depending on the device design, a 5° uncertainty in the contact angle from contact-angle hysteresis leads to $\sim 6\ \mu$m of uncertainty in the contact-line position [6]. In order to reduce the hysteresis and have a reasonable actuation voltage, a thin layer of hydrophobic coating of Teflon AF2400 was used [22].

In the fourth step of the fabrication process, a two-step recipe was used for spin-coating of Teflon AF2400:

i) 500 RPM speed with 100 RPM acceleration for 5 seconds,

ii) 3000 RPM speed with 1000 RPM acceleration for 30 seconds.

Next, the Teflon layer is baked on a hot plate at three steps: first 7.5 minutes at 115°C, then 5 minutes at 245°C, and finally 15 minutes at 305°C.

Patterning of the Teflon AF2400 hydrophobic layer was carried out in two steps. First, the patterns were defined by photolithography using level-4 photomask. The photoresist used for this aim was mixed with a surfactant (Zonyl FSN) in two different configurations: i) 90 vol% AZ5214E PR - 10 vol% Zonyl, ii) 95 vol% AZ5214E PR - 5 vol% Zonyl. The use of a surfactant is necessary since it is impossible to coat PR on Teflon without it. Also, coating of the PR on a pre-heated wafer enhances the adhesion of it to the wafer [40].

Spin-coating of the PR was done in two steps: First, the wafer was heated to 110°C on a hot plate for 5 minutes and then the PR mixture with 10 vol% Zonyl content was spin-coated at 4000 rpm with acceleration of 2000 rpm for 40 seconds without waiting for the wafer to cool down. Next, the PR was soft-baked at 110°C for 50 seconds. At the second step, the PR mixture with 5% Zonyl content was spin-coated with the same parameters, again without cooling of the wafer. After another soft-bake at the same temperature, the PR was exposed to UV light with constant dose (175 mJ) using the forth mask.

Development of the PR was carried out using AZ400K developer (AZ400K:H_20 = 1:2) for 60 seconds. After development, the Teflon layer was etched for 45 seconds with Oxygen Plasma in ICP system with 100 sccm oxygen flow. The power values used were 400 W 13.56 MHz for RF coil and 20 W 13.86 MHz for platen. The resulting Teflon layer thickness was about 100 nm. Figure 3.13 shows the sample device with coated and patterned Teflon hydrophobic layer.

3.1.6 Coating and Patterning of SU-8 Layer

The fifth and final step in the fabrication process is the coating and patterning of the SU-8 layer. This 400 μm-thick layer serves as the container of the metal droplet used in the device for switching purposes. Moreover, SU-8 layer makes it possible to position the droplet with high accuracy.

The negative photoresist SU-8 3050 from MicroChem was coated on the wafer

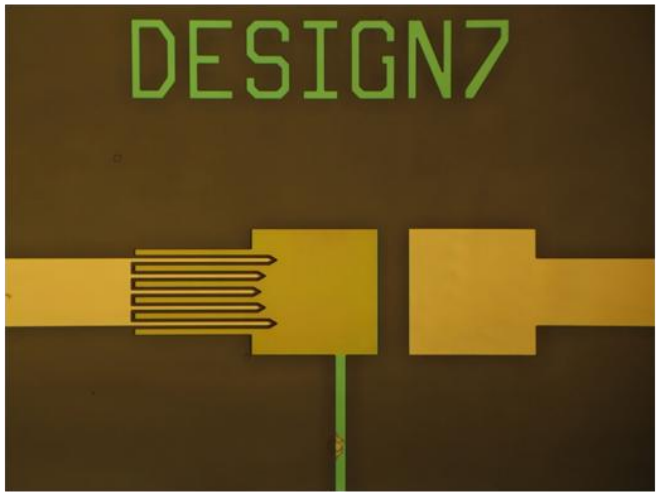

Figure 3.13: Sample device with coated and patterned Teflon AF2400 hydrophobic layer.

using a two-step spin coating process: 500 RPM speed with 100 RPM acceleration for 5 seconds as the first step, and 1000 RPM speed with 100 RPM acceleration for 30 seconds as the second step. 400 μm thickness was not reached in one shot: first, a 100 μm-thick layer was spin-coated and then soft-baked on a hot plate at 95°C for 45 minutes. After baking and cooling in air for 10 minutes, the process was repeated as many times till the desired thickness value was achieved. In our case, this process was repeated 4 times to reach $\sim$ 400 μm.

The SU-8 layer was exposed to UV in mask aligner with constant dose of 1200 mJ in proximity mode with 30 μm separation. The reason for using proximity mode was sticking of the SU-8 coated wafers to the mask. Despite trials with different baking parameters, this problem could not be prevented. Thus, exposure was carried out using the proxy mode of the mask aligner. Additionally, exposure dose was increased from 1000 mJ (in soft contact mode) to 1200 mJ (in proximity mode). After exposure, a post exposure bake step was carried out on a hot plate at 100°C for 20 minutes. Finally, the SU-8 photoresist was developed for 60 minutes using mr-Dev 600 developer from Micro Resist Technology. Hard-bake of the resist is optional. The fabricated sample device and whole wafer containing devices with different parameters are shown in Figure 3.14 and Figure 3.15, respectively.

Also, Figure 3.16 shows the whole microfabrication process schematically.

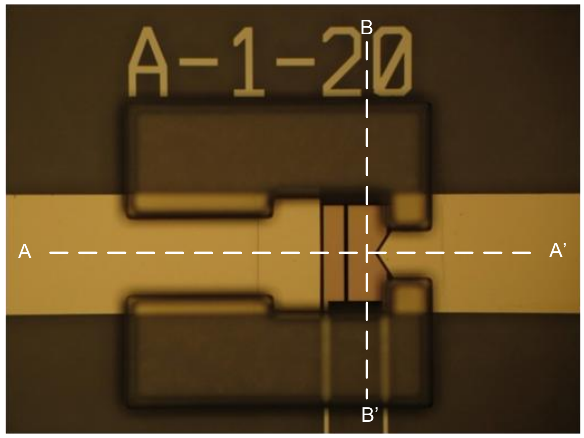

Figure 3.14: Optical microscope image of a completed LS-MEMS test device.

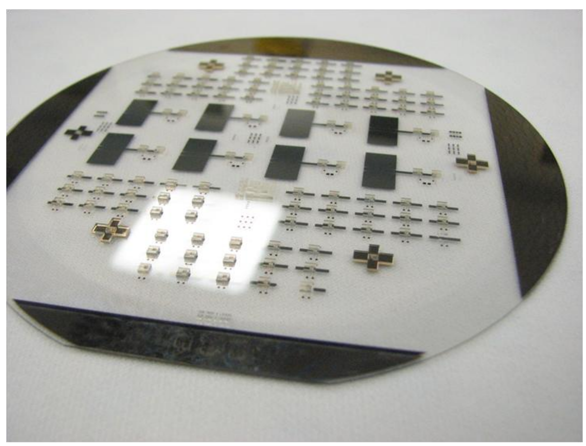

Figure 3.15: Completed wafer after 5 mask-level microfabrication process including 98 LS-MEMS switch devices.

Figure 3.17 shows the photomasks as designed using L-Edit software. The figure shows all 5 mask layers. During photomask preparation process, all but one mask layer are hidden and the visible layer is exported as Graphic Database System (GDS) file. Then, that layer is written to the photomask by making use of Heidelberg Instruments DWL-66 Laser Mask Writer.

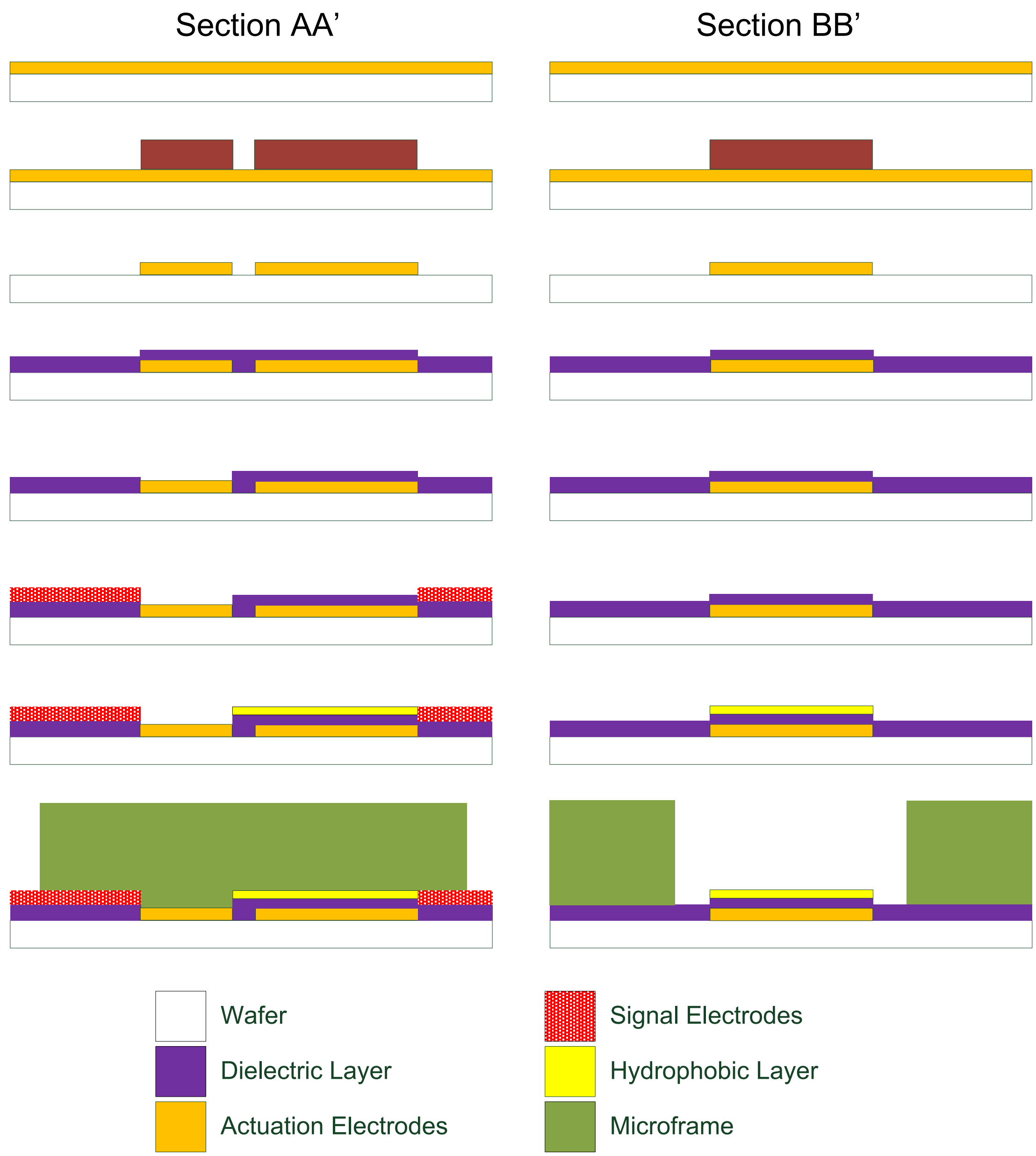

Figure 3.16: Microfabrication steps of LS-MEMS devices. Section AA' and Section BB' are shown in Figure 3.14.

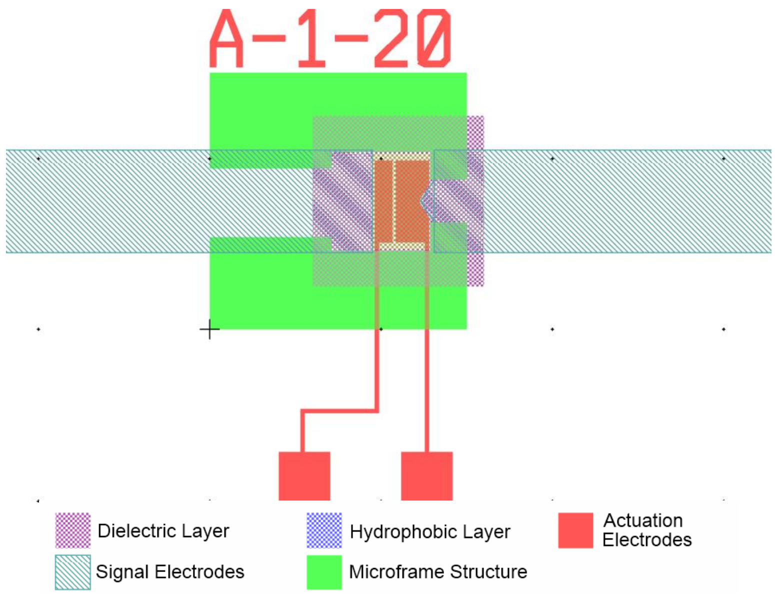

(a)

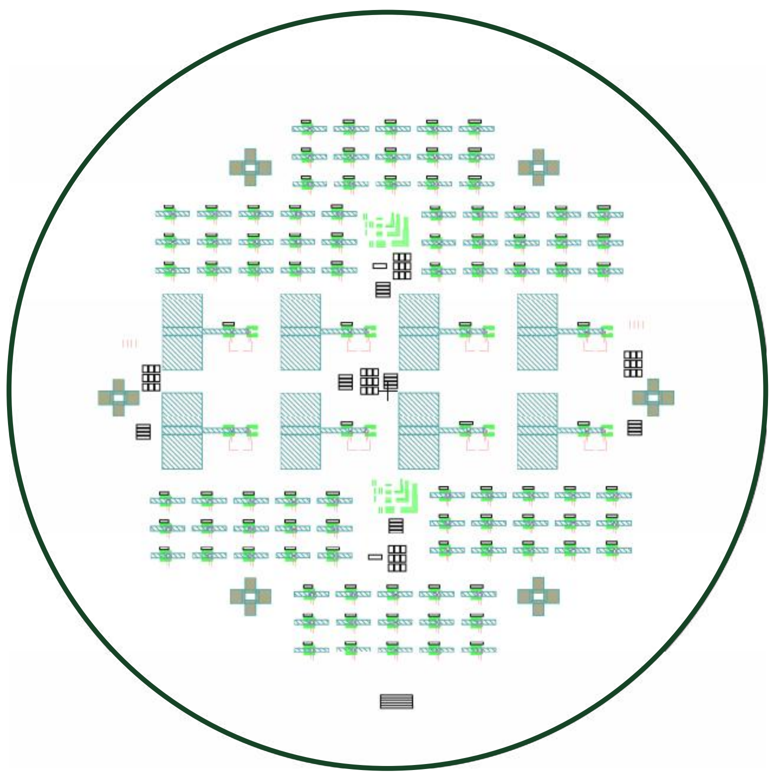

(b)

Figure 3.17: Design of the photomasks used in this work. The design was drawn in L-Edit software (a) single device, (b) full-wafer mask design.

3.2 Characterization Setup

At the beginning of the fabrication process, coating processes of different layers with different materials were optimized utilizing various physical vapor deposition equipments. The thicknesses of coated layers were measured with KLA Tencor surface profiler (Figure 3.18). Also, spectroscopic ellipsometer was used for the characterization of coated PECVD SiO_2 layers. Another characterization step of the test devices involved visual inspection with optical microscope and FEI-brand Nano-SEM (Figure 3.19 and Figure 3.20).

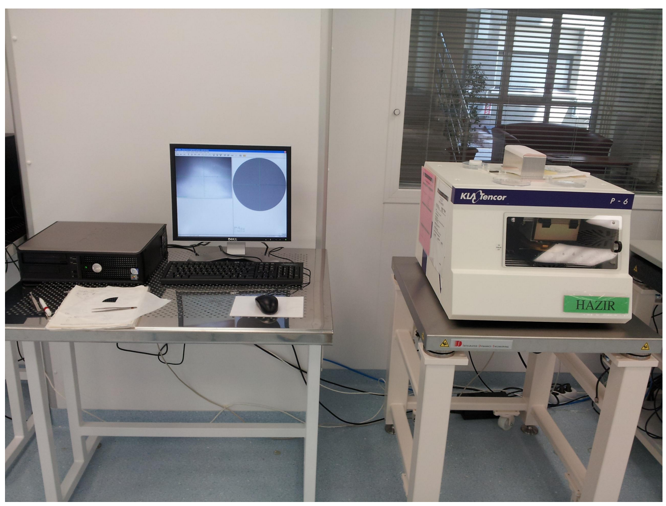

Figure 3.18: KLA Tencor surface profiler utilized for thickness measurements.

Confirmation of the optimum initial contact angle of the droplets are especially important, since a higher contact angle allows application of a higher actuation force to a droplet, as explained in the previous chapter. That's why contact angle measurements of DI-water and metallic droplets on hydrophobic surfaces are carried out using Dataphysics OCA 30 (Figure 3.21).

During the experiments, three different metallic liquids have been used: Mercury (Hg), Eutectic Gallium Indium (EGaIn) and Gallium Indium Tin alloy (Galinstan). The droplets are positioned manually on the devices and then probed in the probe station (Figure 3.22(a)). The experiments are carried out on different

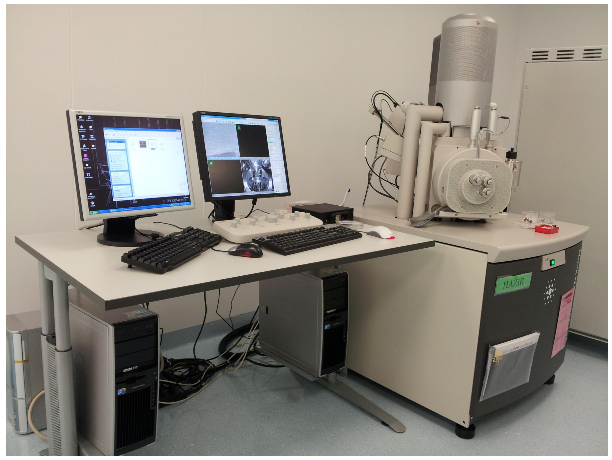

Figure 3.19: FEI-brand Nano-SEM was used for SEM imaging of the test devices.

devices on the same wafer as can be seen in Figure 3.22(b). Every device on the wafer differs from others by its dimensions and geometry. A test device with the deposited mercury droplet is shown in Figure 3.22(c).

The schematic representation of a completed test device is shown in Figure 3.23. Actuation experiments are carried out under a Cascade Microtech electrical probe station connected to a Keithley 4200-SCS parameter analyzer. The actuation voltage was applied on probe 1 and ground was applied on probe 2, which is also the signal-in electrode. Meanwhile, probe 3 touched the signal-out electrode and 3 V was applied on this probe. As a consequence of the device design, the liquid droplet always touched the ground electrode. Voltage was applied between signal-in and signal-out electrodes with the purpose of sensing if the droplet touched also the signal-out electrode when it is actuated. With the application of voltage between the actuation electrode and ground electrode, charge distributions in the droplet and the dielectric changed, causing a decrease in surface tension. This led to spreading of the droplet portion at the smaller opening of the microframe structure and movement of the contact line forward on actuation electrode. In this state, the switch was on. When application of the potential was stopped, the contact line moved back to its original position and the switch became off.

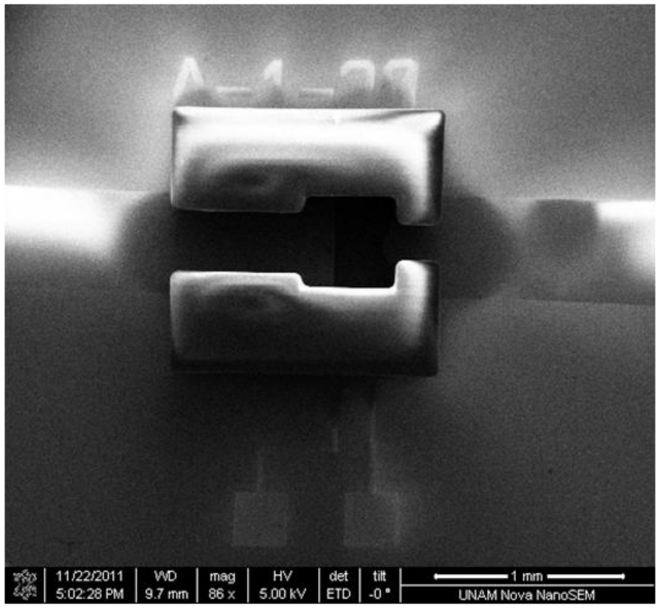

Figure 3.20: Visual inspection of a fabricated device utilizing SEM.

Figure 3.21: Equipment used for contact angle measurements throughout this work.

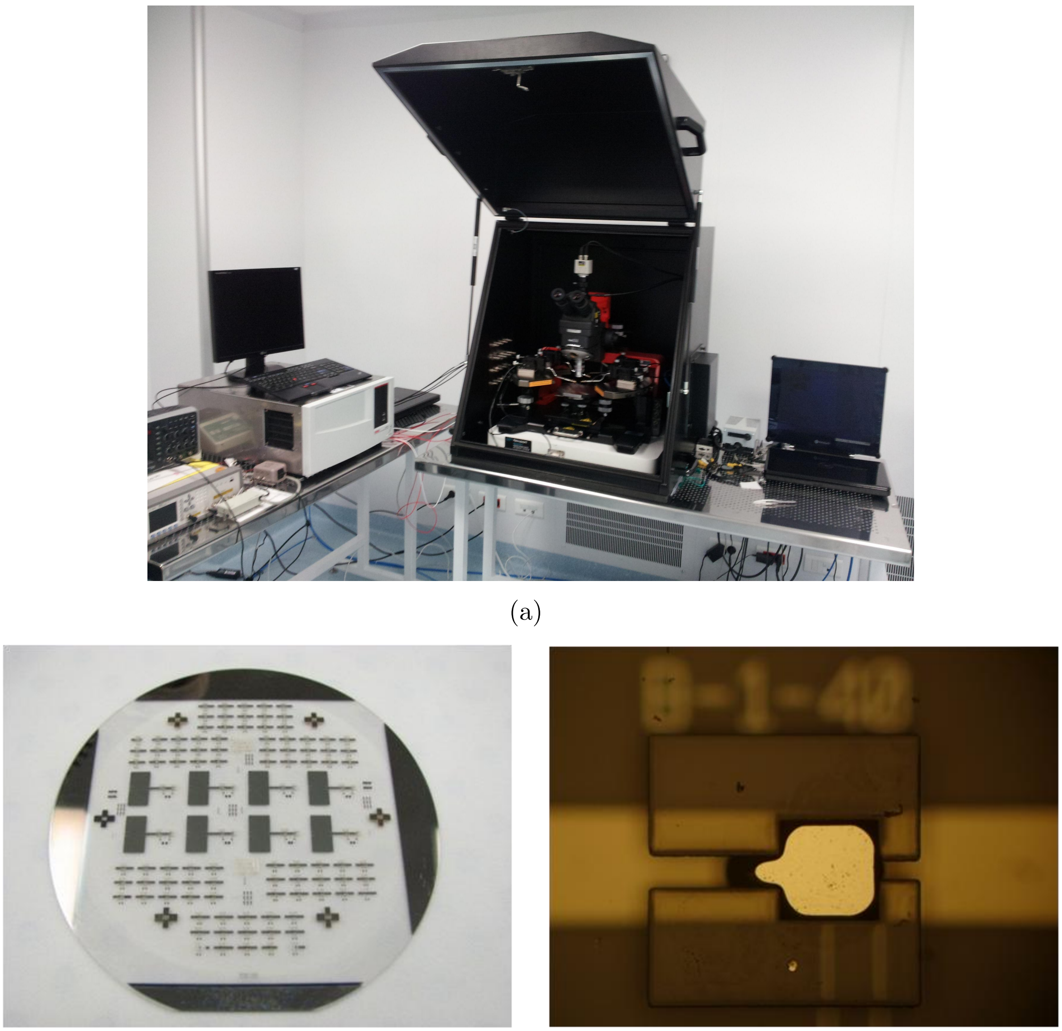

(a)

(b) (c)

Figure 3.22: (a) The experimental setup used in this work: a probe station connected to a parameter analyzer; (b) a fabricated 4-inch quartz wafer with 98 test devices; (c) A test device with a positioned metallic droplet.

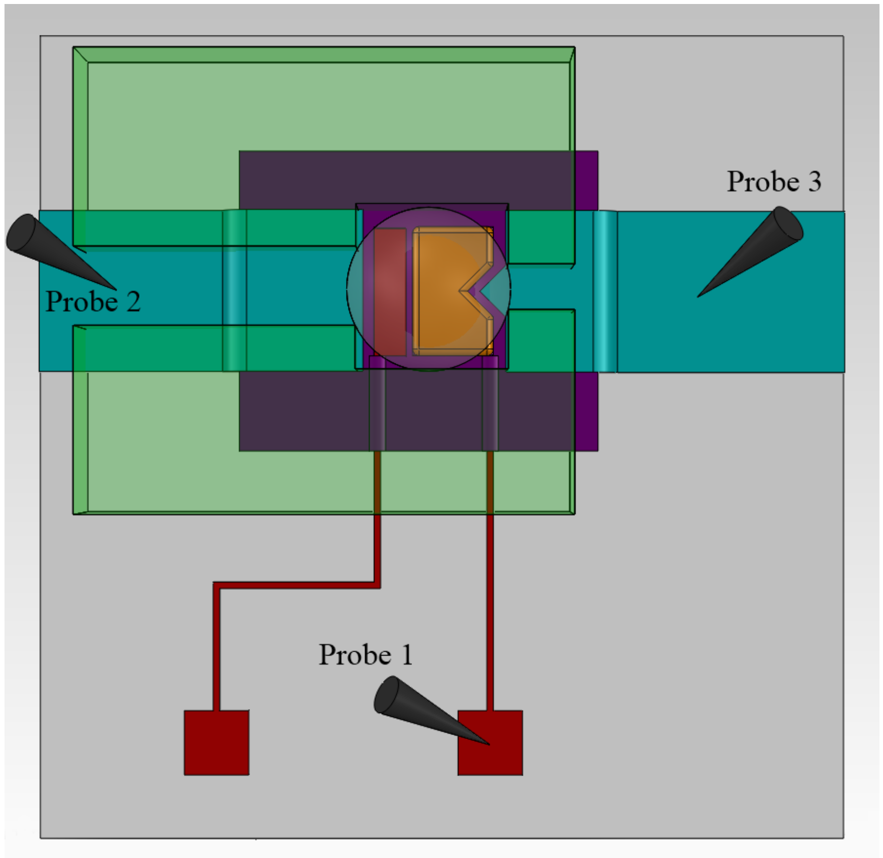

(a)

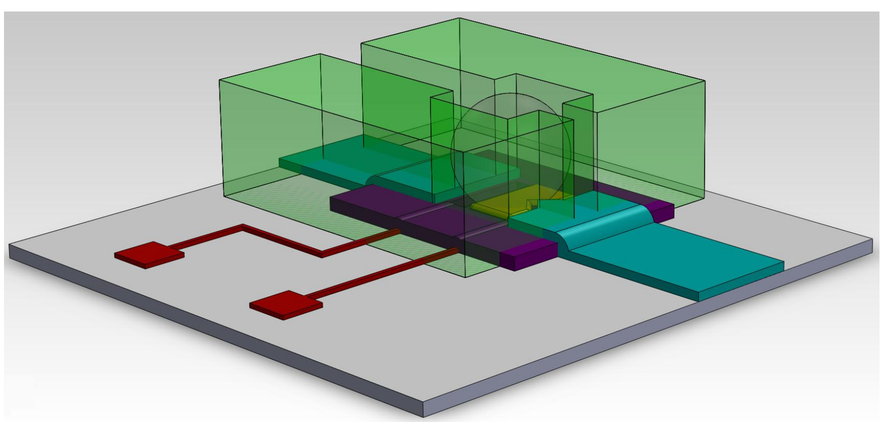

(b)

Figure 3.23: (a) Schematic representation of a completed test device from top view during an experiment, which shows the electrodes to which the probes touch. (b) Schematic drawing showing an LS-MEMS device with its layers and a positioned liquid metal droplet.

Chapter 4

Results and Discussion

In this chapter, results of switching experiments using liquid-solid microelectromechanical (LS-MEMS) metallic droplet-based switches are presented. Furthermore, it is demonstrated that room-temperature liquid metal alloy droplets of EGaIn and Galinstan alloy can be actuated using EWOD effect. With the application of 30-100 V voltage difference between the actuation electrode and the ground electrode, the metallic liquid droplets were observed to be actuated. Actuation experiments with and without thick SU-8 wall structures, different dielectric thicknesses, different dielectric materials including SiO_2, Al_2O_3, and HfO_2, different droplet materials (mercury, EGaIn and Galinstan) and different droplet sizes were carried out. The initial results show that a systematic experimental optimization of the LS-MEMS switches might provide an alternative technology for high-performance RF-switching applications.

Throughout this thesis work, various LS-MEMS devices have been designed to examine different device geometries and materials. Among the electrode materials deposited in different devices, chromium, aluminum, and gold were used. The dielectric layers utilized included silicon dioxide (SiO_2), hafnia (HfO_2), alumina (Al_2O_3) and layered combinations of them. During experiments, two different hydrophobic layers, TMMMA (Perfluoro Methacrylate Methyl Methacrylate) and Teflon AF2400 from DuPont were used.

Actuation experiments in closed-pack microfluidic channels were also successful with slightly higher actuation voltages. We attribute this result to the partial adhesion of liquid-metal droplets to the SU-8 walls, especially at the corners. The effect of dielectric layer thickness on the actuation voltage was studied as well. Thinner high-k dielectric layers resulted in lower actuation voltages as low as 30 V.

4.1 Contact Angle Measurements

As stated in Chapter 3, the aim of coating a hydrophobic layer on top of the dielectric layer is to get the optimum initial contact angle during droplet actuation. In order to ensure a minimum contact angle of 120°, a series of coating experiments were carried out with two different hydrophobic coating materials: TMMMA consisting of 20 mol% TM (Perfluoro Methacrylate) and 80 mol% MMA (Methyl Methacrylate), and Teflon AF2400. A device with the TMMMA hydrophobic layer is shown in Figure 4.1. The contact angle of the droplet is measured to be 104.8°, which is lower than the targeted value.

Figure 4.2 shows the contact angle measurements of DI-water droplet on Teflon AF2400 hydrophobic layer. The measured contact angle is 130.1°, which corresponds to a higher value compared to TMMMA. Therefore, in the succeeding devices, Teflon was chosen as the hydrophobic coating material.

For process simplicity, the idea of coating PR as the hydrophobic layer was tested. Figure 4.3 shows the contact-angle measurement of DI-Water on AZ 4533-coated surface, which is 69.8°. As can be deduced from the measurement, it brings no benefits to use PR as a hydrophobic layer.

As can be seen from Figure 4.4, Galinstan and EGaIn droplets on Teflon-coated surfaces formed distinctively non-spherical shapes. According to the work of Dickey et al., this results from the fact that both droplets form a skin of gallium oxide after even a brief exposure to air. They used Auger spectroscopy to analyze samples of EGaIn. Results showed an enhanced amount Ga and O at the surface

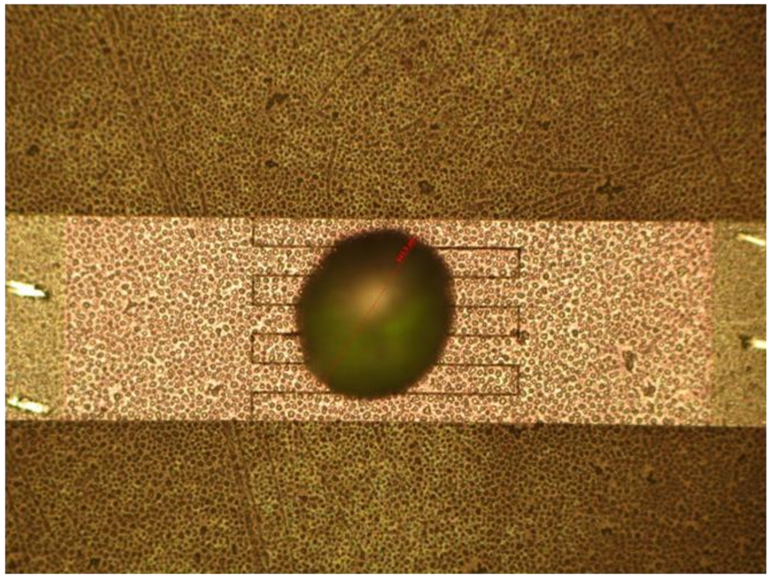

Figure 4.1: An LS-MEMS device with TMMMA hydrophobic layer.

(atomic % ratio In:Ga:O = 1:15:17) compared to the bulk, suggesting that the skin primarily consists of oxides of gallium. Moreover, they reported that the oxide skin forms a highly uniform passivation layer that protects the bulk material from further oxidation [17]. Contact angles of Galinstan and EGaIn were measured to be 110.9° and 134.6°, respectively. However, these values were not reliable and estimated contact angles depend on the shape of the droplets, since they have non-spherical shapes.

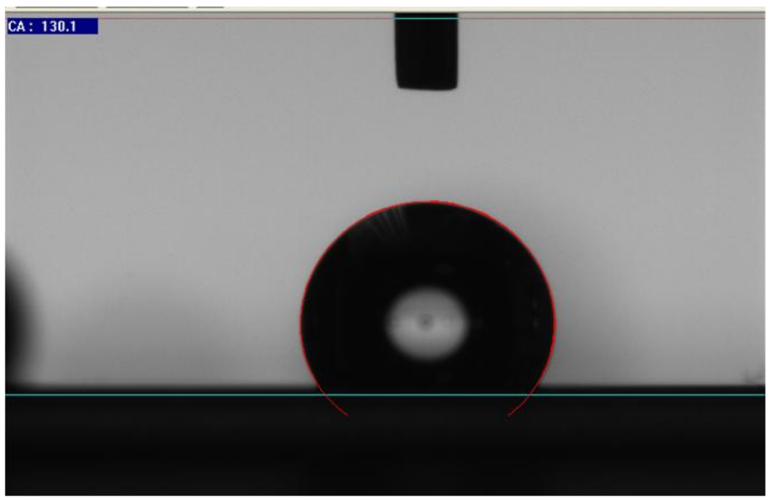

Figure 4.2: Contact-angle measurement of DI-water on Teflon-coated surface.

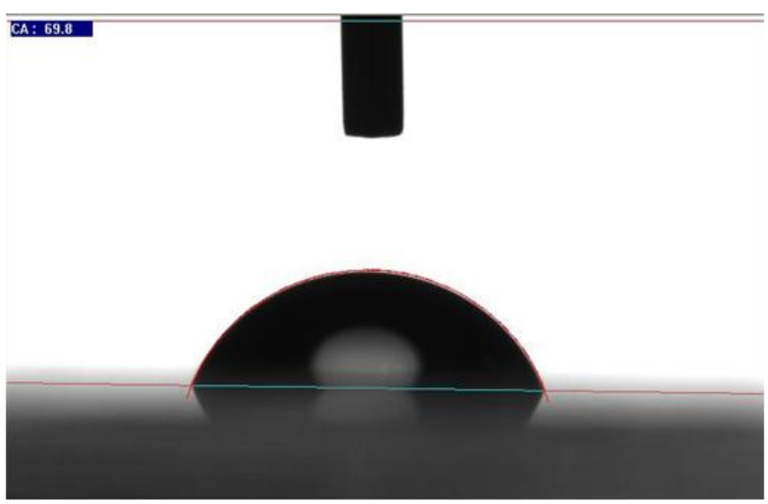

Figure 4.3: Contact-angle measurement of DI-water on AZ 4533-coated surface.

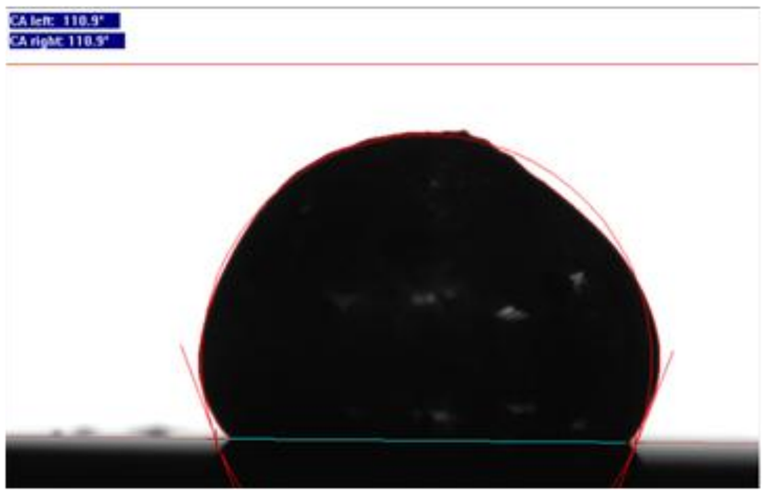

(a)

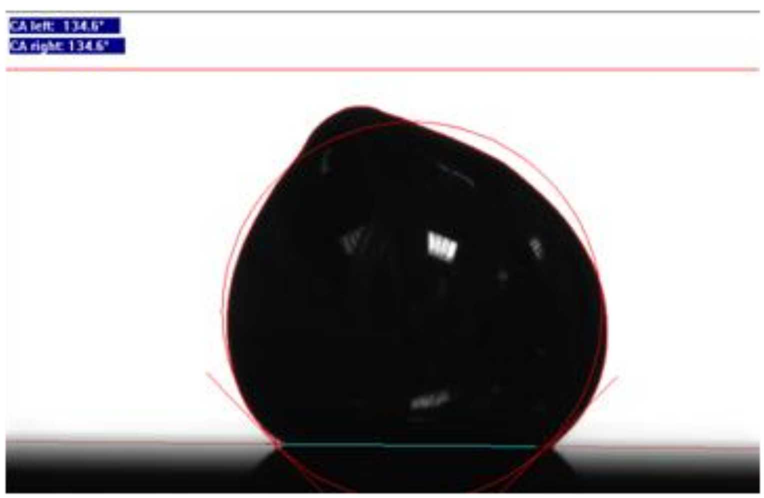

(b)

Figure 4.4: Contact-angle measurement of (a) Galinstan (b) EGaIn on Teflon-coated surface.

4.2 Proof of Concept Devices

The first generation of LS-MEMS switches consisted of thermal evaporated 10/100 nm-thick Cr/Au electrodes and 300 nm-thick PECVD-grown SiO_2 dielectric layer (Figure 4.5). The sole purpose of these devices with interdigitated fingers was to prove that the mercury droplets could be actuated and moved.

In the experiments done with droplets of mercury and DI-water, it was observed that with the application of >60 V actuation voltage the droplets moved towards the actuated electrode. Moreover, an increase in the applied potential resulted in the increase in droplet velocity and decrease in latency, as expected.

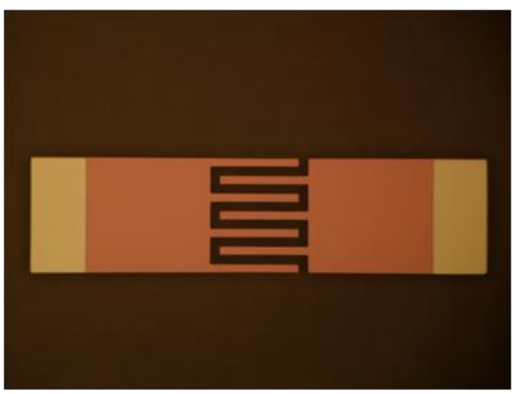

(a)

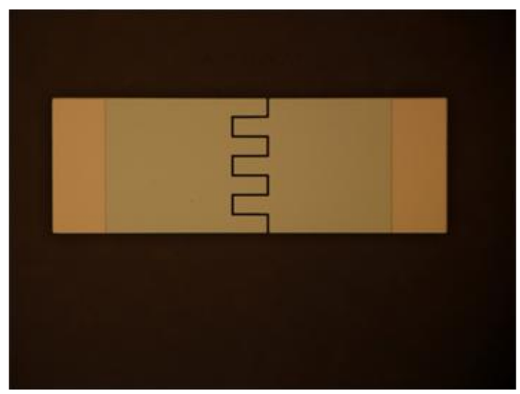

(b)

Figure 4.5: First generation of the LS-MEMS devices with interdigitated fingers.

4.3 Droplet Position Optimization

One of the important parameters for successful droplet actuation is the amount of droplet overlap over the actuation electrode (Figure 4.6). In general, to a certain extend, the higher the overlap, the higher the applied actuation force. In order to optimize the force applied on the droplet during actuation, a series of experiments with different amounts of overlap were carried out. Observations showed that, an overlap of at least 40% resulted in successful and repeatable actuation. Below that overlap amount, the applied force was not high enough to actuate the droplet. Above 80% overlap, on the other hand, the actuation force was observed to decrease.

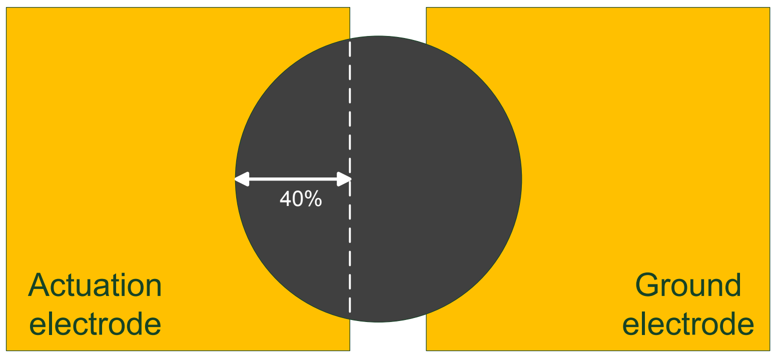

Figure 4.6: Schematic top view of a droplet with 40% overlap.

4.4 Devices with Ground Electrodes

Experiments with first generation LS-MEMS switches revealed that devices without a ground electrode have limited actuation ability and show repeatability problems because of the charge saturation in the liquid droplet which resulted in lower applied net force on the droplet, as explained in [8]. Therefore, second generation devices with separate ground electrodes were designed and fabricated using a two-mask microfabrication process. There were two types of them; those with ground electrodes on the same level as actuation electrodes (Figure 4.7) and those with ground electrodes over the SiO_2 dielectric layer (Figure 4.8).

First generation of devices was successful in the actuation of mercury droplets. With the application of >80 V potential difference between the metal electrode and the droplet, the droplet was actuated and moved towards the electrode.

Although a few successful experiments were carried out with the second generation of devices, most of them resulted in the electrical breakdown of the oxide dielectric layer. While they had the same level of fabrication complexity as

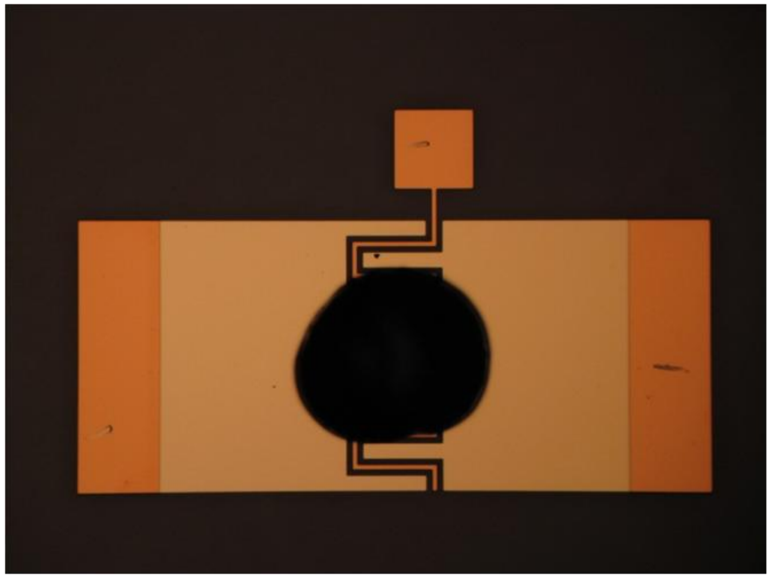

Figure 4.7: An interdigitated LS-MEMS device with ground electrodes (line in-between right and left electrodes) on the same level as actuation electrodes. The droplet shown in the figure is an EGaIn liquid metal droplet.

the first type, during the experiments, the second type of devices suffered from the breakdown of the ground lines and the 300 nm-thick oxide dielectric layer (Figure 4.8(c) and Figure 4.8(d)). The main reason was that the oxide could not withstand the high electric field density resulting from the high applied voltages (>80 V). This problem might be solved by using a high-k material as the dielectric layer, such as Al_2O_3 or HfO_2 instead of SiO_2 as in the work of Chang et al. [7], or by changing the device design.

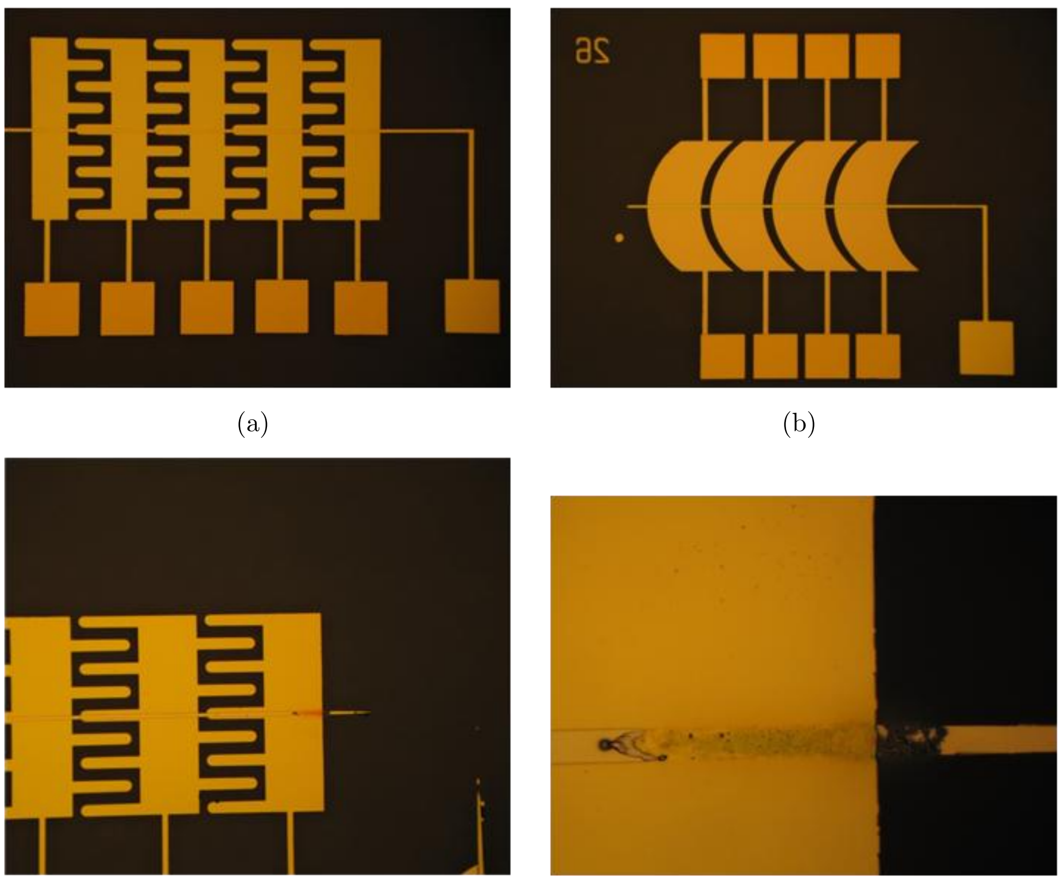

(a) (b)

(c) (d)

Figure 4.8: Optical microscope images of devices with ground electrodes over the dielectric layer: (a) Devices with interdigitated fingers; (b) Devices with crescent-shaped electrodes; (c) Failure because of high electric field density; (d) Close-up look of the failure.

4.5 LS-MEMS Switches with SU-8 Microframe

The use of a microframe in LS-MEMS devices brings advantages such as accurate positioning of the droplet, thus ease of droplet deposition, and stability under acceleration, which prevents any unintended switching. Accordingly, LS-MEMS devices with 400 μm-high SU-8 microframe structures were fabricated. SU-8 is in fact a negative tone photoresist, so it can be patterned by photolithography. During fabrication, SU-8 2075 and SU-8 3050 from MicroChem with a thickness of 100 μm at a spin-coating speed of 1000 RPM were used. Moreover, during exposure a dark field mask was used to pattern them. Although SU-8 3050 is much easier to work with, both SU-8 types require fine optimization of the process parameters including baking temperatures, exposure dose and development time.

The microframe structure used had asymmetrical openings (Figure 4.9). While because of surface tension, any excess or shortage in the deposited-droplet volume is compensated by the meniscus deformation at the bigger opening (right side), the meniscus at the smaller opening (left side) does not change, so that the liquid-solid contact line remains more-or-less at the same position. The pressure needed to move the interfaces should be considered to explain the reason. A higher pressure is required for a meniscus to move in a smaller opening compared to that in a larger opening. This means that any change in the droplet volume will be consumed to move predominantly the right meniscus [6].

Figure 4.10 shows a closer look to the meniscus in the smaller opening of the LS-MEMS device. In addition to the mercury droplet, there is some oil to observe the effect of the letter to the droplet actuation. The meniscus of the oil can be seen as a black line at the left side of Figure 4.10.

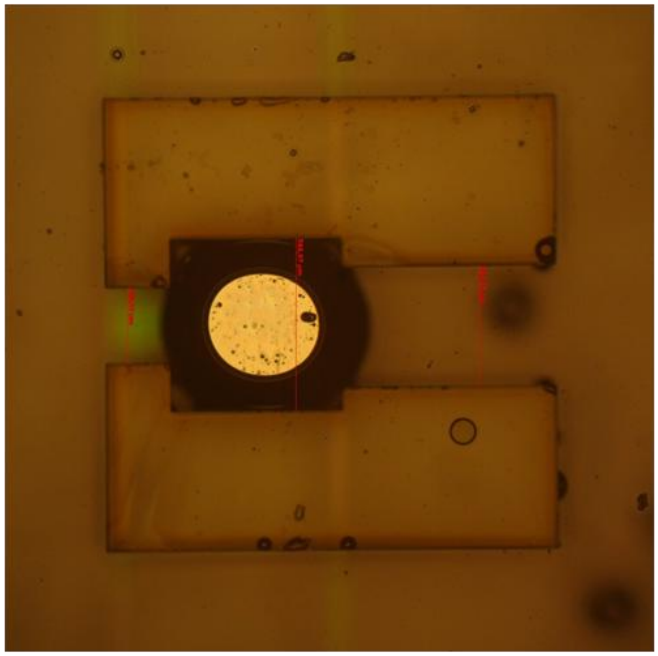

Figure 4.9: LS-MEMS device with the microframe structure having asymmetrical openings.

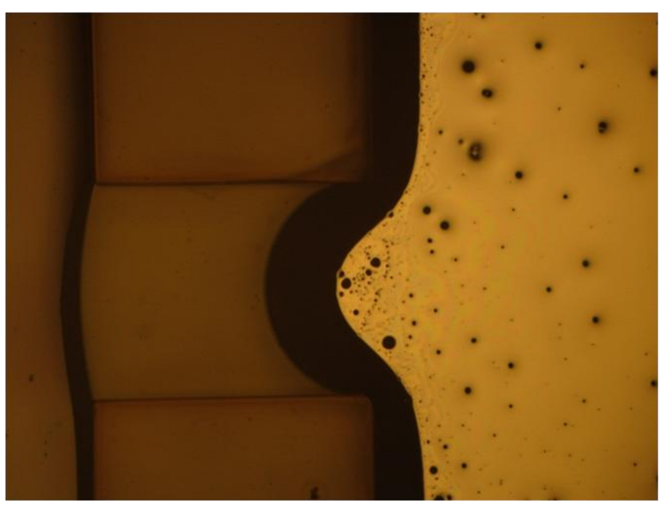

Figure 4.10: Droplet meniscus in the smaller opening of an LS-MEMS switch.

4.6 LS-MEMS Switches with SU-8 Microframe - Merge & Separation

One of our MEMS switch designs made use of a novel idea: MEMS switches with liquid-liquid contacts. Using this design, repeatability and reliability problems seen in solid-solid (and sometimes liquid-solid) switches might be overcome. The proposed design after fabrication and with positioned droplets can be seen in Figure 4.11 and Figure 4.12, respectively. The design makes use of two symmetrical containers for two liquid droplets. Also, electrodes with interdigitated fingers are replaced by rectangular electrodes, since in the former the insulator may easily be subject to voltage breakdown because of sharp voltage contours created [2].

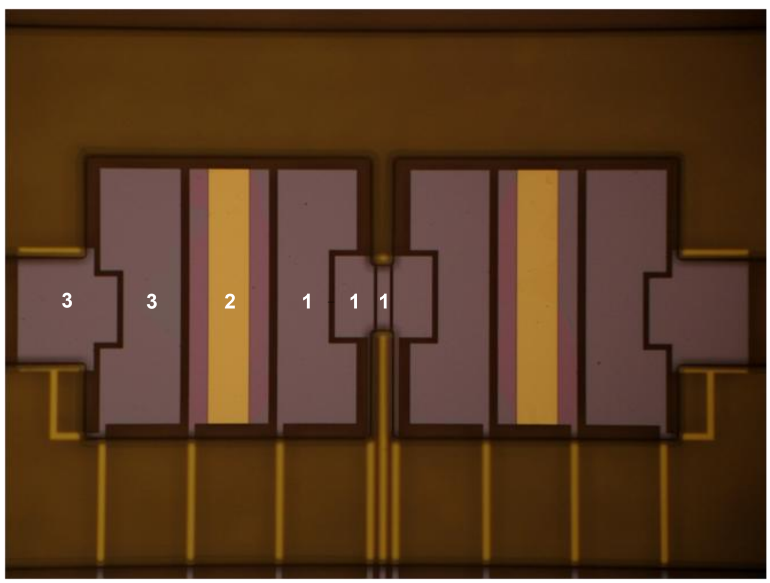

Figure 4.11: Optical microscope image of the fabricated device designed for droplet merging and separation experiments.

As shown in Figure 4.11, there were three groups of electrodes used to actuate the droplets. Group 1 is used to actuate the droplets towards the contact region in the center. Group 2 is the ground electrodes used create an electric field for actuation and also prevent charge saturation in the droplet. Finally, Group 3 electrodes are designed to separate the merged droplets and turn the switch in off state. In the first experiments with this device type, after actuation by applying voltage between the electrode types 1 and 2, the droplets merged (Figure 4.13). During the experiments, the droplets were enclosed using a top glass.

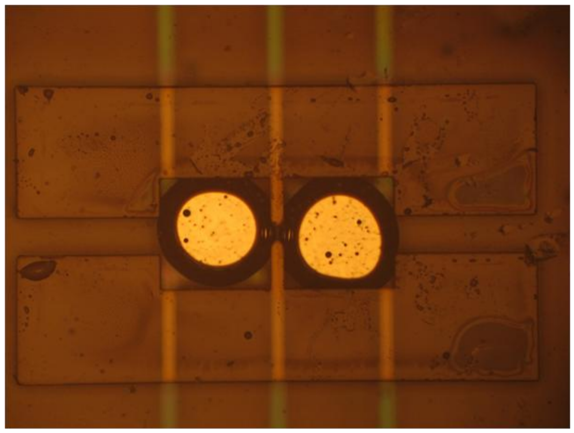

Figure 4.12: Optical microscope image of positioned droplets on a fabricated device used for merge and separation experiments.

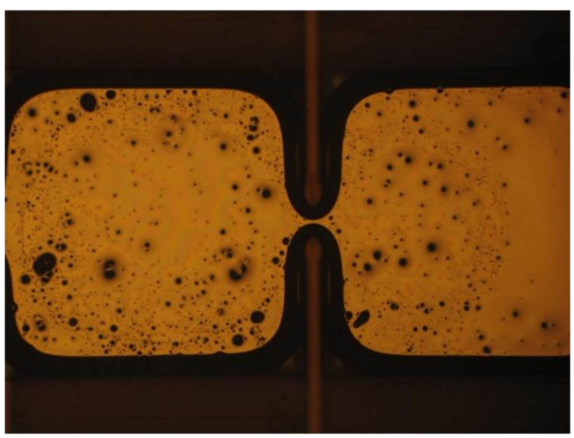

Figure 4.13: Optical microscope image of the fabricated device with positioned and merged droplets.

The black dots seen in the Figure 4.13 stem from the dirt on the top glass and some possible oil left over from the previous experiments. However, they do not affect either the actuation of the droplets or current passing through them.

In the dark field optical microscope images shown in Figure 4.14, the area just inside the green parts of the droplet correspond to the contact line.

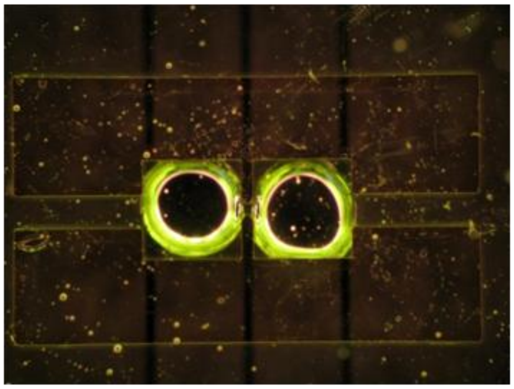

(a)

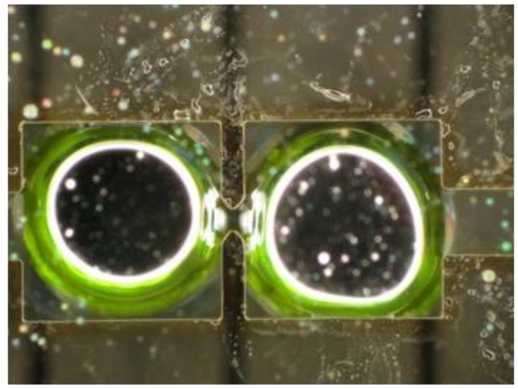

(b)

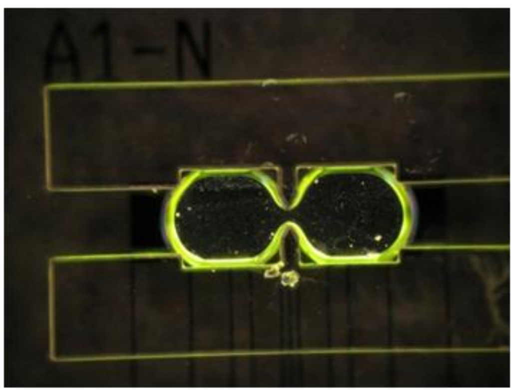

(c)

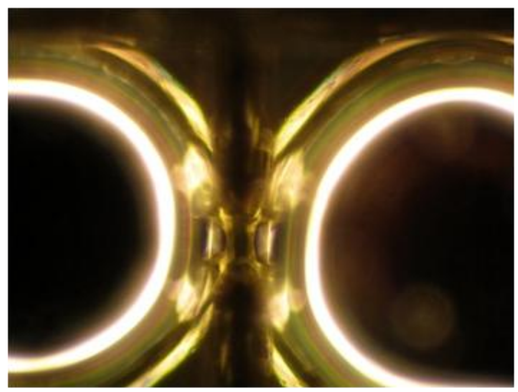

(d)

Figure 4.14: Dark field optical microscope images of positioned droplets on a fabricated LS-MEMS device used for merge and separation experiments.

Because mercury has a high surface tension (435 mN/m), when the droplets touch each other and merge, it requires a higher force to separate the two droplets. In an effort to realize switches with merging and separating mercury contacts, devices were designed with different geometries, such as the one shown in Figure 4.15. The design principle behind the shown device was that as the neck region gets narrower, it becomes easier to separate the already-merged droplets. However, even with this design, we were not able to separate the droplets. One possible reason might be the insufficient back opening preventing enough displacement for the separation of the droplet. Another variable for successful separation is the width of the neck region. As the neck gets narrower, it became easier to separate the droplets, but with a trade-off: it also becomes harder to merge them. Therefore, future work might focus on the optimization of the neck region and the back opening to enable switches utilizing liquid-liquid contacts.

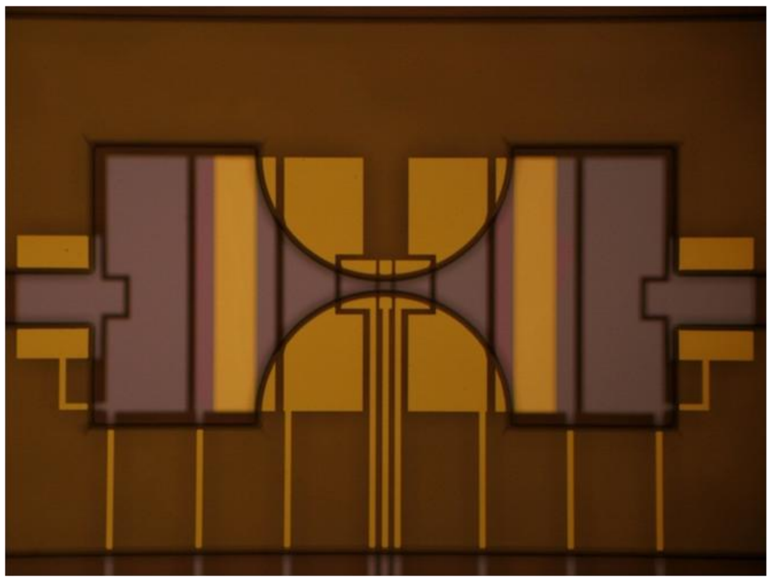

Figure 4.15: Optical microscope image of the fabricated LS-MEMS device having a graded neck region.

Another reason for the failure in the separation of the droplets is the frequent breakdown of the SiO_2 dielectric layer. Although a minimum applied voltage of 100 V is sufficient to actuate and merge the droplets, separation experiments with bias voltages up to >200 V was not successful. At such high values, a significant stress was imposed on the dielectric layer and the dielectric could not withstand the stress resulting in the breakdown of the dielectric (Figure 4.16).

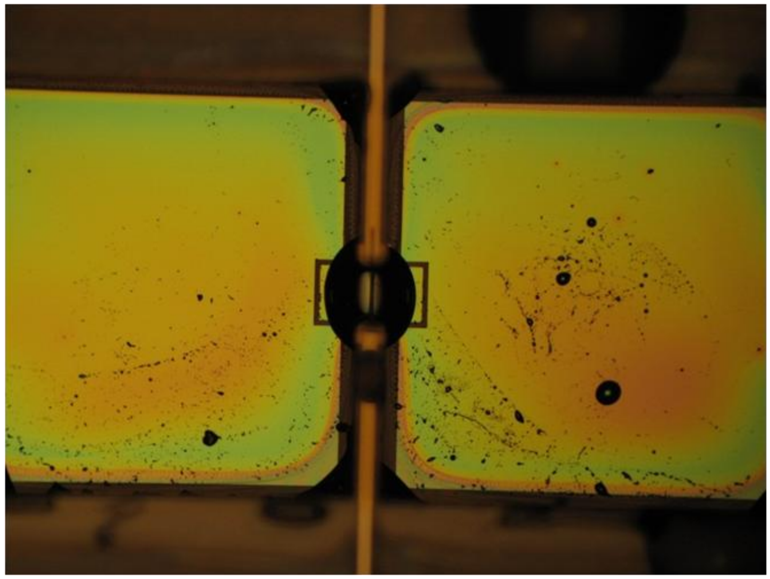

Figure 4.16: Oxide breakdown observed during actuation experiments.

As stated above, a higher pressure is required for a meniscus to move in a smaller opening compared to that in a larger opening. This fact can also be seen from actuation experiment shown in Figure 4.17. In this figure, the Group 3 actuation electrodes, i.e., near the larger openings, are actuated. The outcome is larger distance travelled by the droplet, as expected.

(a)

(b)

Figure 4.17: LS-MEMS switch droplet actuation experiments (a) before actuation, (b) after application of 100 V.

4.7 Inline LS-MEMS Switches

The next generation devices were designed to be used as in-line MEMS switches using a liquid metal droplet as the active switching element (Figure 4.18). The fabrication of the device was a 3-mask-level microfabrication process. For the initial testing purposes only, the electrodes and contact lines were fabricated, the SU-8 layer was not coated. The details of the fabrication process were explained in Chapter 3. First, Cr was sputtered and patterned to define the actuation electrodes. The next step was the deposition and patterning of the SiO_2 dielectric layer. Then, signal lines were defined by image reversal photolithography, and after sputtering of Cr/Ni material, lift-off was carried out. Finally, a 100 nm-thick Teflon layer was spin-coated and baked.

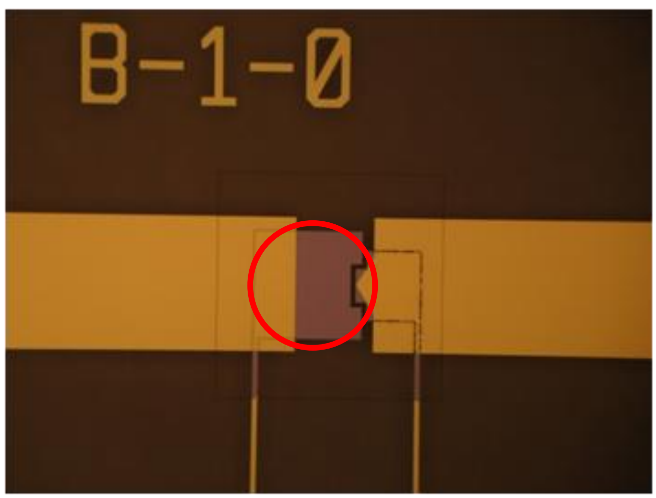

Figure 4.18: Position of the droplet after the actuation is shown by the red circle.

During the experiments, a droplet was positioned in a way to touch only the left (signal-in) electrode of the device. When the droplet was actuated using the right electrode by applying <60 V actuation voltage, it moved to the right and closed the switch by touching both signal electrodes (the ON state of the switch) as shown by a red circle in the Figure 4.18. When a potential was applied between the left electrode and the droplet, the droplet moved to the left making the switch off. However, because the 300 nm-thick SiO_2 dielectric layer could not withstand the electric field, most of the experiments ended with dielectric breakdown (black lines seen in Figure 4.19(a)-4.19(c)).

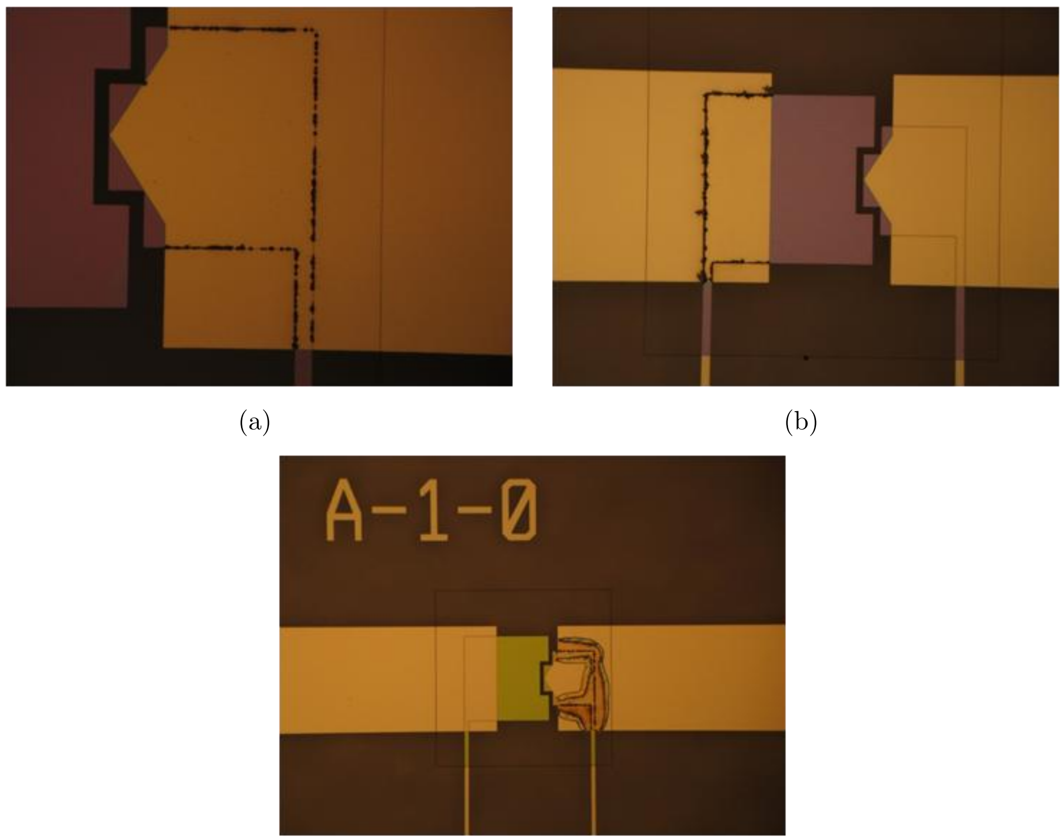

(a) (b) (c)

Figure 4.19: Failure of the LS-MEMS devices because of dielectric breakdown.

The failure of the devices above led to a different design approach, as shown in Figure 4.20. In this new design, the actuation electrodes did not overlap with the signal lines. Moreover, there was a 10 μm lateral separation between the electrodes and the lines. As a result, the dielectric thickness between them was increased to 10 μm, which could withstand potentials higher than 210 V, which is maximum voltage that could be applied using the Keithley 4200-SCS parameter analyzer. Moreover, the shape of the actuation electrode allowed applying a higher actuation force throughout droplet motion.

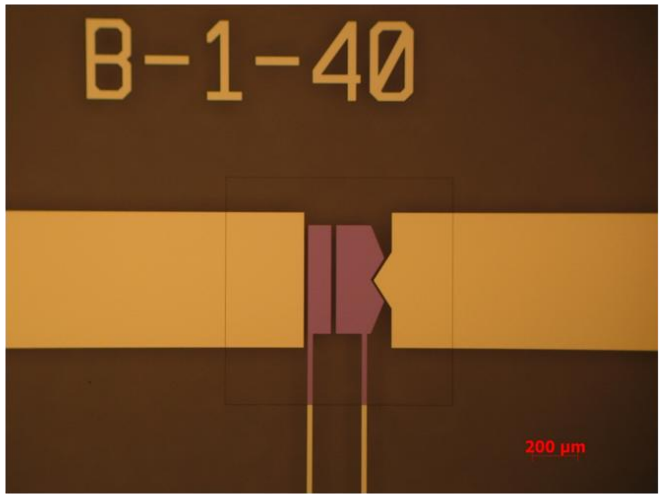

Figure 4.20: New LS-MEMS design with the actuation electrodes not overlapping with the signal lines.

4.8 Teflon Hydrophobic Layer Patterning

The use of a hydrophobic layer makes it necessary to perform a fabrication process to pattern it. The reason is that the microswitch design in this work requires DC contact between the liquid metal droplet and the signal electrodes. When the hydrophobic layer is not patterned, however, this requirement is not met.

To satisfy the need of Teflon hydrophobic layer patterning, several approaches have been taken. The first one was the lift-off patterning of the layer. In this approach, first, the final pattern was defined on a 1.4 μm-thick AZ 5214 photoresist by image reversal photolithography using a light field mask. Then, the Teflon layer was spin-coated and baked at 120°C, the highest possible temperature when photoresist is present, for 10 minutes. After lift-off in acetone overnight, the Teflon patterns were generally not as desired, as shown in Figure 4.21. This stems from the fact that the photoresist is not thick enough to remove the undesirable Teflon regions. Lift-off process requires the photoresist to be thick enough to make an elevation difference so that the unwanted material over the photoresist is taken away.

Figure 4.21: Unsuccessful Teflon patterning (Lift Off). Photoresist used was AZ 5214 with a thickness of 1.4 μm.

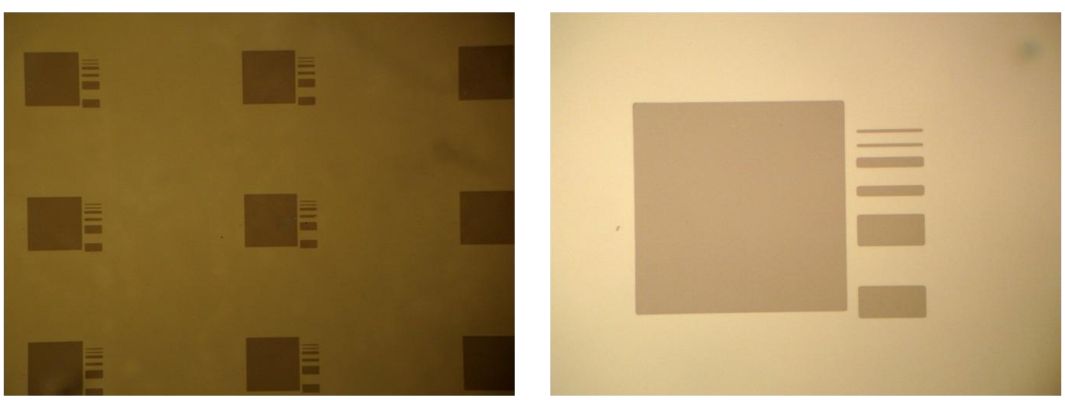

(a)

(b)

Figure 4.22: (a) Teflon Patterning (Lift Off). Photoresist used was AZ 4533 with a thickness of 3.3 μm. (b) Close-up look of the patterned Teflon layer.

In the second approach, a 3.8 μm-thick photoresist (AZ 4533) was used. The photomask used during fabrication was dark field, since AZ 4533 is a positive tone photoresist. Following the same fabrication processes the Teflon patterns were much better, as shown in Figure 4.22. Using the second approach, devices with patterned Teflon layers were able to be fabricated (Figure 4.23). However, there also existed a significant number of devices with fabrication defects such as shown in Figure 4.23(c). Additionally, during actuation experiments with these devices, the droplets tended to stick on the Teflon layer, most probably due to the degradation of Teflon.

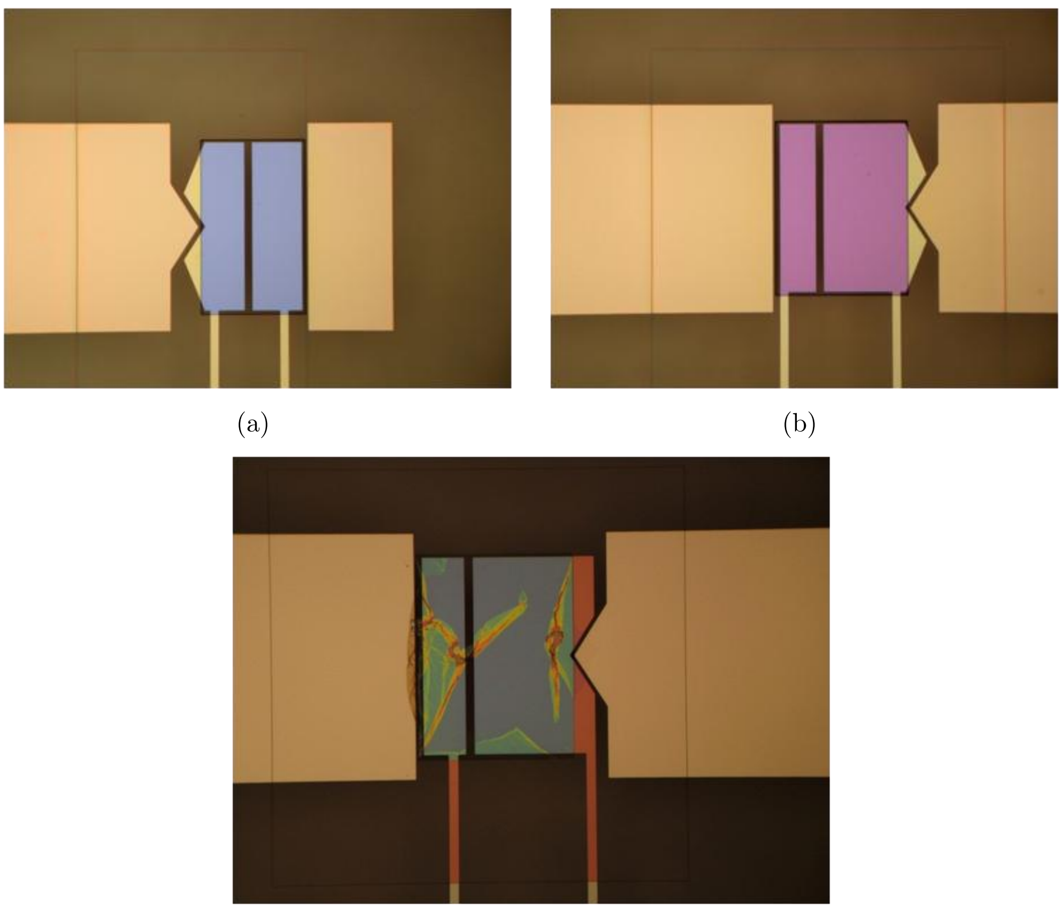

(a) (b)

(c)

Figure 4.23: (a), (b) Completed LS-MEMS devices with patterned Teflon layers; (c) A device with fabrication defects.

The yield in the second approach was also not as high as expected. Over ten devices fabricated, nearly four were patterned well. The reason behind the patterning problems seen in both approaches was the relatively low Teflon baking temperature during the process. Teflon is known to have weak mechanical bonding to the substrate, when baked at temperatures lower than specified in its datasheet (110°C, 245°C, and 315°C in successive baking steps) [41]. The proper baking of Teflon is prohibited by the presence of photoresist in the process, since when photoresists are baked at temperatures higher than 150°C, it becomes very hard to remove them from the substrate surface [42].

Experiments so far led to the conclusion that another approach to Teflon patterning problem was needed. Since Teflon does not allow coating of any solution on top of it as a result of its chemical nature, the first two approaches used lift-off as the patterning strategy. This rules the choice of first coating Teflon on the substrate and then patterning it using photoresist out. However, as stated in the work of Cho et al., the use of a surfactant, namely Zonyl FSN, makes it possible to pattern the already coated Teflon layer [40]. For this purpose, experiments with both Zonyl FSA and Zonyl FSN were carried out.

In the experiments with both Zonyl types, first the Teflon layer was spin-coated and baked according to the procedure in the datasheet. Then, a certain vol% Zonyl-added AZ 5214 photoresist was spin-coated and baked with usual photoresist processing parameters. After exposure with an etching mask using various UV exposure doses in different experiments, the Zonyl-added photoresist is developed. The resulting photoresist film in the case of 20 vol% Zonyl FSA is shown in Figure 4.24. Using this Zonyl type, a patterned photoresist film suitable for Teflon patterning could not be achieved.

In the experiments with Zonyl FSN from Sigma Aldrich, a two-step photoresist coating process was carried out. For this purpose, two different Zonyl-photoresist mixtures were prepared: First with 10 vol% Zonyl FSN and 90 vol% AZ 5214 mixture, second with 5 vol% Zonyl FSN and 95 vol% AZ5214 mixtures. After coating and baking of the Teflon hydrophobic layer, the wafer was heated to 110°C at the hot plate. Immediately after taking the wafer from the hot plate,

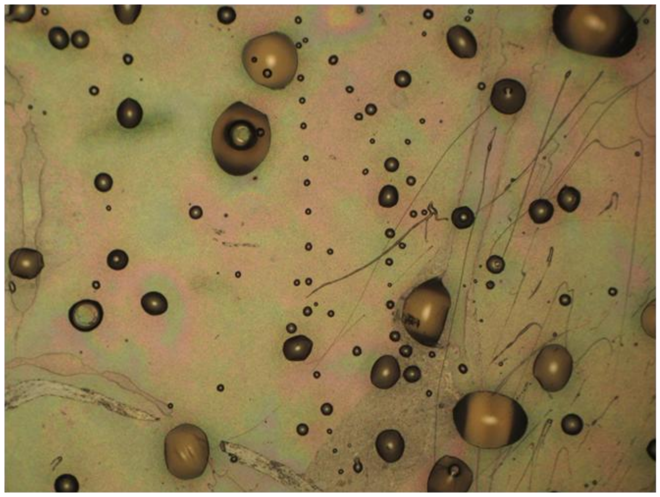

Figure 4.24: Development of 20 vol% Zonyl FSA added AZ 5214 Photoresist.

without allowing it to cool down, the photoresist mixture with 10 vol% Zonyl FSN was spin-coated. After soft baking for 50 seconds at 110°C at the hot plate, again without allowing it to cool down, the second mixture with 5 vol% Zonyl FSN is spin coated. Another soft-bake is carried out with same parameters and the photoresist was exposed to UV with a dose of 75 mJ. After 3 minutes of development using AZ400K developer (AZ400K:H_20 = 1:5), the desired patterns did not appear. Figure 4.25 shows three regions in the processed wafer: at the top the photoresist is developed, in the middle a partially developed region can be seen and finally at the bottom an undeveloped region exists.

Compared to the case with Zonyl FSA, Teflon patterning using Zonyl FSN as the surfactant was more promising. However, the latter required optimization of the photolithography process parameters. As a result of a dozen of photolithography trials with different exposure doses, developer mixture ratios and development times, the optimum process parameters were found to be 175 mJ exposure dose, AZ400K developer (AZ400K:H_20 = 1:2) and 60 seconds development time. These parameters enabled coating and patterning of a photoresist layer on top of an already spin-coated Teflon layer. The Teflon layer was etched for 40 seconds in Inductively Coupled Plasma (ICP) system using the patterned photoresist layer as a soft mask. The result is shown in Figure 4.26.

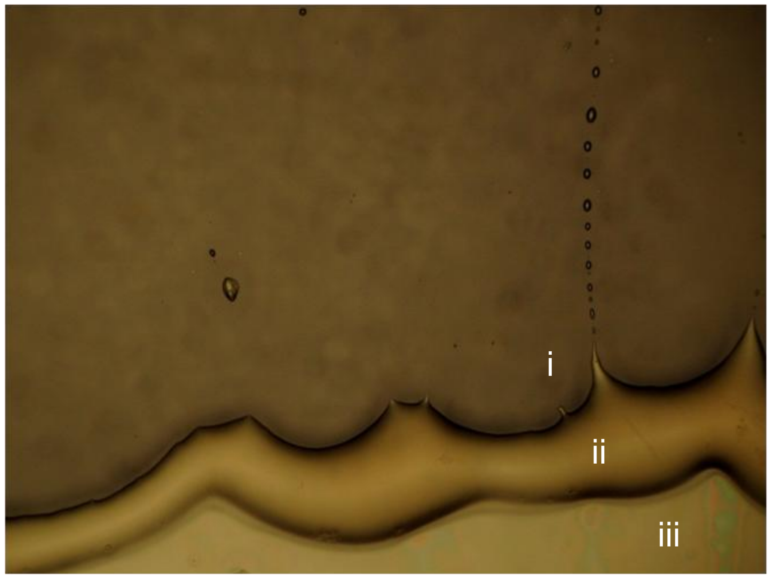

Figure 4.25: Three regions in the processed wafer: i) at the top the photoresist is developed, ii) in the middle a partially developed region can be seen, and finally iii) at the bottom an undeveloped region exists.

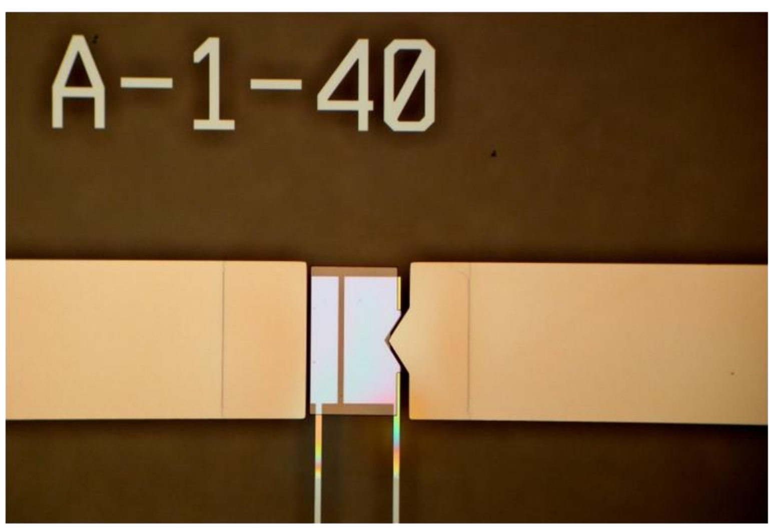

Figure 4.26: Successful patterning of the Teflon AF layer using Zonyl FSN as the surfactant with optimized photolithography parameters.

4.9 Final Generation of LS-MEMS Devices

Using the former device experience and taking into account the advantage of the ability to pattern the Teflon hydrophobic layer, a new LS-MEMS switch structure was designed. Figure 4.27(a) shows an optical microscope image and Figure 4.27(c) shows a SEM image of the new device. Moreover, Figure 4.27(b) shows a device with positioned droplet with a glass top cover.

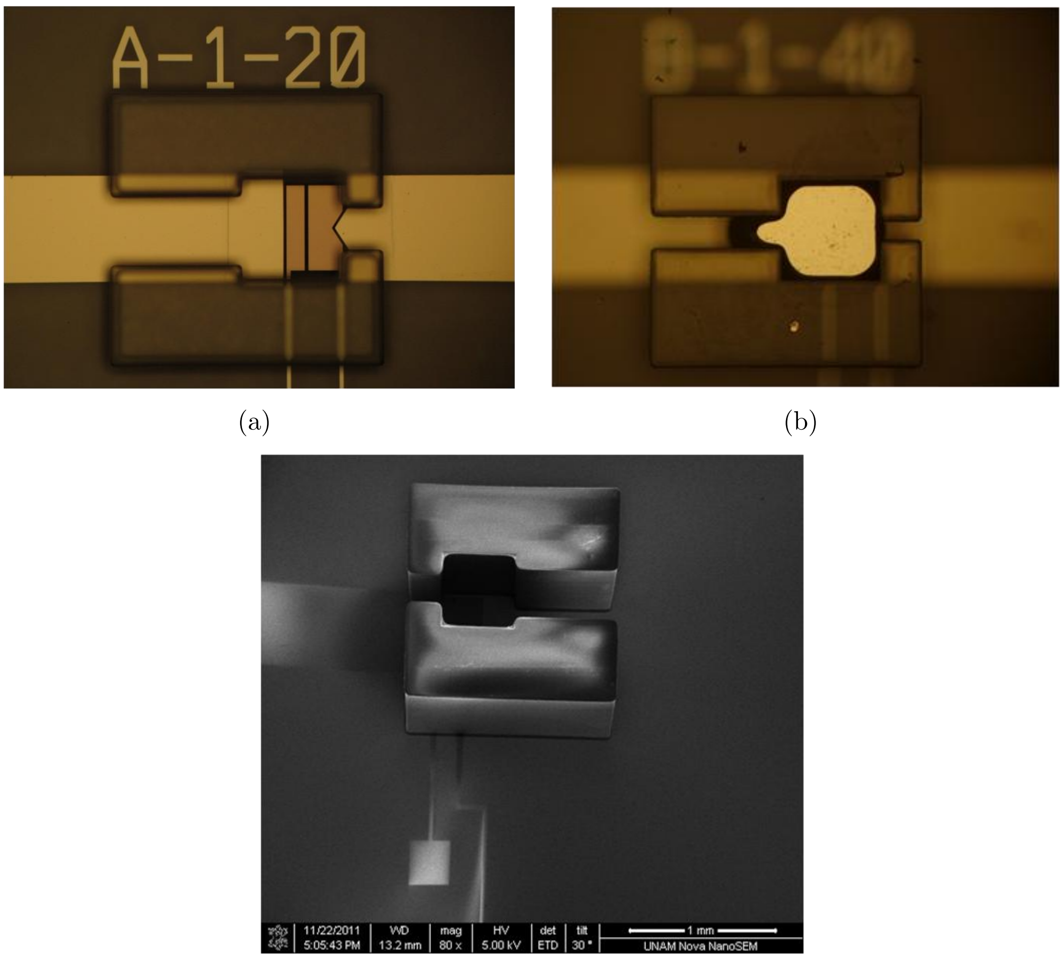

(a) (b)

(c)

Figure 4.27: Optical microscope image of a fabricated LS-MEMS device (a) without and (b) with the positioned droplet with a glass top cover. (c) Angled SEM micrograph of the fabricated LS-MEMS device.

During the experiments carried out using devices with this new design, three major problems arose. In the first case, the switch was made on after successful droplet actuation, but the droplet did not draw back after the application of voltage was stopped. As a result, the switch stayed always on. We propose that there might be two possible causes for this: i) Due to the adhesion of the liquid droplet on the SU-8 walls, the droplet gets stuck and no movement is possible. This can be overcome by utilizing a new SU-8 design that positions the droplet by touching it only at the corners. That way, minimum amount of contact can be achieved preventing adhesion of the droplet. ii) Charging of the dielectric layer during actuation. In this case, charges trapped inside the dielectric apply an electric field although application of the potential is stopped. This applies electrostatic force on the droplet preventing it from drawing back. According to the work of Sen et al., although the failure due to short-term dielectric charging was solved by biasing the mercury positive [35], a problem of long-term dielectric charging still exists and will lead to device failure like all other capacitively driven MEMS switches [6].

Secondly, the droplet did not move enough and failed to turn the switch in ON-state. Again, this may be due to the adhesion of the liquid droplet on the SU-8 walls and can be overcome by utilizing a new SU-8 design that positions the droplet by touching it only at the corners. Another reason may be the insufficient applied force on the droplet. As discussed earlier, the force applied on the droplet can be increased by increasing the capacitance of the system, i.e., either by coating a dielectric layer with higher dielectric constant or decreasing the thickness of the dielectric layer or both.

The third major problem was related to the repeatability and droplet stiction due to dielectric failure. As can be seen from Figure 4.28, during experiments with some test devices the SiO_2 dielectric layer failed to sustain the high electric field. The reason for this result might be the poor quality of PECVD SiO_2 featuring pin holes which might lead to early electrical breakdown of the devices.

Table 4.1 shows voltages applied during experiments to different devices on the same wafer. The devices differ from each other by the distance the contact

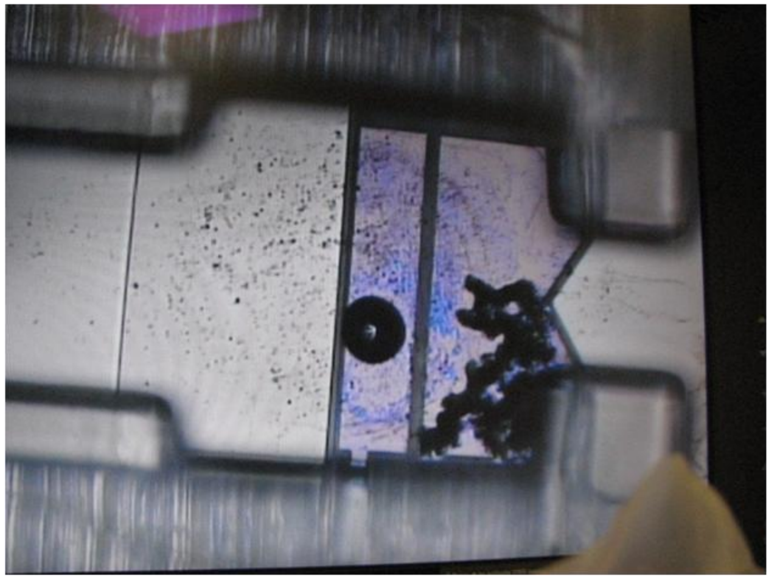

Figure 4.28: Dielectric failure and mercury residue in a test device.

line of a droplet has to travel to close the switch. For example, A-1-0 denotes the reference device. A-1-20, on the other hand, means that the signal-out electrode is 20 μm closer to the droplet. Therefore, it has to travel 20 μm less to close the switch. The aim of varying the position of signal-out electrode is to determine the optimum position which realizes repeatable switching.

Table 4.1: Actuation voltages applied to different LS-MEMS devices on the same fabricated wafer

Run	**A-1-0**	**A-1-120**	**C-1-20**
1	80 V	80 V	80 V
2	120 V	120 V	120 V breakdown
3	180 V breakdown	160 V	
4		210 V	

During actuation experiments, liquid metal droplets were positioned manually. The applied voltage was increased starting from 80 V to 210 V, the highest voltage the parameter analyzer can apply. As can be seen in Table 4.1, dielectric layer

(SiO_2) of A-1-0 broke down at 180 V. After failure, the device looked like as shown in Figure 4.28. Although in device A-1-120 a voltage as high as 210 V was applied, the droplet could not close the switch. In C-1-20, the SiO_2 dielectric layer broke down at a lower voltage, 120 V.

4.10 Final Generation of LS-MEMS Switches with High-k (Hafnia + Alumina) Dielectric Layers

As stated at the end of previous section, the force applied on the droplet could be increased either by coating a dielectric layer with higher dielectric constant or decreasing the thickness of the dielectric layer or both. Dielectric layer of devices in that section was SiO_2 material with a dielectric constant of 3.9. Results of the experiments with previous device led to another device design in which the dielectric layer consisted of HfO_2 (hafnia) and Al_2O_3 (alumina) (Figure 4.29). The choice of these two materials stems from their high dielectric constants (25 and 9 for hafnia and alumina, respectively).

The dielectric consisted of a 30 nm alumina layer on top of a 30 nm hafnia layer. For hafnia layer, the precursor used was Tetrakis(dimethylamido)hafnium, $Hf(NMe_2)_4$. During deposition, the coating parameters used were: 200°C deposition temperature, 0.015 seconds H_2O pulse, and 0.2 seconds $Hf(NMe_2)_4$ pulse, resulting in a deposition rate of 1.01 Å/cycle. Therefore, hafnia layer was coated for 300 cycles to achieve $\sim$ 30 nm thickness. For alumina layer, Trimethylaluminum (TMA) was the precursor used. During deposition, the coating parameters used were: 200°C deposition temperature, 0.015 seconds H_2O pulse, and 0.015 seconds TMA pulse, resulting in a deposition rate of 1.05 Å/cycle. So, hafnia layer was coated for 300 cycles to achieve $\sim$ 30 nm thickness. Patterning the two dielectric layers required the use of ICP equipment in the UCF. The recipe used for alumina etching had the following process parameters: Cl_2 and Ar process gases, 5 mTorr pressure, 200 W 13.56 MHz coil power, and 50 W 13.56 MHz

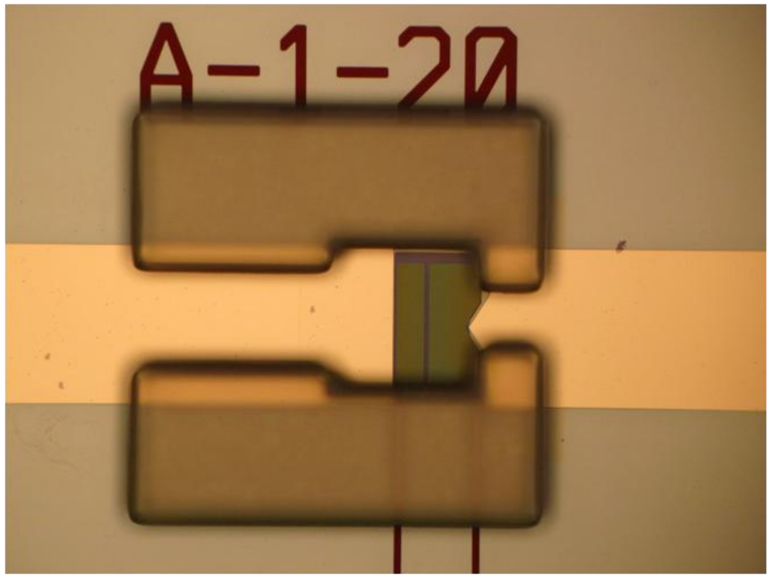

Figure 4.29: LS-MEMS switch with hafnia and alumina layers as the dielectric.

platen power. On the other hand, a physical etch process with argon plasma was used in order to pattern the hafnia layer. Initial tests without the SU-8 layer resulted in mercury droplet actuation voltages as low as 30 V, much less than obtained with 300-nm-thick SiO_2.

As discussed earlier, devices utilizing dielectric layers with higher dielectric constants result in higher capacitance and therefore, lower actuation voltages. Table 4.2 shows the actuation voltages of droplets in devices without SU-8 microframe. The two devices had SiO_2 and hafnia + alumina as dielectric layers. As can be seen, the second type of devices exhibited lower actuation voltages.

Table 4.2: Actuation voltages of liquid droplets in LS-MEMS devices where the dielectric layer is SiO_2 and hafnia + alumina

Dielectric	**Actuation Voltage**
SiO_2	>60 V
hafnia + alumina	>30 V

In this device generation, the dielectric layer broke down at voltages around 80 V. Despite successful droplet actuation without SU-8 microframe at >30 V, in the presence of the microframe, the droplet actuation attempts were partly unsuccessful. In devices with SU-8 microframe, the droplets were actuated, however, the contact line could not travel enough distance to turn the switch in ON position. The possible reason was adhesion of the liquid droplet on the SU-8 walls, in which case the droplet gets stuck and enough droplet movement was not observed.

Chapter 5

Conclusions and Future Directions

In this study, design, fabrication, and material/device characterizations of liquid-solid MEMS (LS-MEMS) devices with liquid metal droplet actuation for electrical switching via electrowetting-on-dielectric (EWOD) principle are demonstrated. Moreover, to the best of our knowledge, the actuation of non-toxic metallic liquid droplets, namely EGaIn and Galinstan, has been studied for the first time. We have investigated the effect of different actuation electrode geometries including rectangular, interdigitated fingers and crescent-shaped electrodes on the droplet actuation.

Throughout this work, first, contact angle measurements of various liquid droplets were carried out on TMMMA and Teflon AF2400 hydrophobic layers to characterize the surface properties of the LS-MEMS switches. The aim of coating a hydrophobic layer on top of the dielectric layer was to get the optimum initial contact angle during droplet actuation. The measured contact angles on Teflon AF2400 meet the requirements for successful droplet actuation, i.e., the contact angles were higher than 120°.

Next, droplet position during actuation was optimized. It was observed that at least 40% overlap with the actuation electrode results in optimum actuation force application on the droplet. Then, initial actuation experiments were carried out utilizing first generation devices with interdigitated finger electrodes.

After successful droplet actuation experiments with > 80 V applied voltage, actuation characteristics were analyzed utilizing LS-MEMS devices with various device architectures. Lessons learned and experience gained from each device design constituted the criteria for the design of the succeeding devices. For instance, in one of the device generations, it was observed that when a signal electrode and the actuation electrode overlap, the dielectric in between cannot withstand the high electric field. Thus, in the succeeding device designs, they were re-designed in such a way that they did not overlap, which increased the thickness of the dielectric between them.

Experiments using Galinstan and EGaIn liquid droplets revealed that they form a skin of gallium oxide after even a brief exposure to air. Contact angles of Galinstan and EGaIn were measured to be 110.9° and 134.6°, respectively. However, these values were not reliable and estimated contact angles depend on the shape of the droplets, since they had non-spherical shapes.

Although very promising, the use of EWOD principle to realize LS-MEMS switches utilizing liquid droplets as the switching element has some challenges stemming from various sources. In an attempt to solve these issues, some future directions that might help to improve the device performance are as follows:

i) Optimization of the SU-8 microframe design. For instance, it can be redesigned so that it can position the droplet by touching it only from a few points instead of a continuous droplet confinement.

ii) Further optimization of PECVD SiO_2 deposition recipe to increase the quality of the layer to solve the repeatability problems due to the dielectric film quality.

iii) Utilization of high-k dielectric layers including HfO_2 and Al_2O_3 might further improve the switching performance by further decreasing actuation voltages with higher reliability. Indeed, our preliminary results showed the effectiveness of using ALD for the coating of high-k dielectric layers, which resulted in significantly decreased actuation voltages down to 30 V.

iv) As detailed in Chapter 4, during experiments with LS-MEMS switches utilizing droplet merge and separation, it was relatively easy to merge the droplets. However, once merged, it was not possible to separate the droplet. Thus, another possible future work might include a detailed physical and mechanical analysis, and simulation of forces acting on the two droplets. As a result, devices with optimum neck region design might be realized.

v) The issues encountered with EGaIn and Galinstan can be solved by avoiding their contact with the atmosphere. For this purpose, experiments utilizing these metallic droplets can be carried out in an inert-atmosphere nitrogen/argon glove box; in which case these oxygen reactant droplets can act as true liquids.

vi) Another important future work to be completed is the detailed RF-characterization (insertion loss and isolation performance), switching response time measurement, and reliability tests of the fabricated LS-MEMS devices.

To conclude, the initial results obtained from this work show that LS-MEMS devices are promising alternative candidates for high-performance electrical switching. A systematic experimental optimization of these novel class of MEMS switches might provide an alternative technology for RF-switching applications.

Bibliography

[1] N. Kumari, V. Bahadur, and S. V. Garimella, "Electrical actuation of electrically conducting and insulating droplets using ac and dc voltages," *Journal of Micromechanics and Microengineering*, vol. 18, September 2008.

[2] N. Rajabi and A. Dolatabadi, "A novel electrode shape for electrowetting-based microfluidics," *Colloids and Surfaces A: Physicochemical Engineering Aspects*, 365, pp. 230-236, 2010.

[3] W. Shen, R. T. Edwards, and C. J. Kim, "Electrostatically actuated metal-droplet microswitches integrated on CMOS chip," *Journal of Microelectromechanical Systems*, vol. 15, no. 4, pp. 879-889, August 2006.

[4] G. Beni and M. A. Tenan, "Dynamics of electrowetting displays," *Journal of Applied Physics*, vol. 52, no. 10, pp. 6011-6015, October 1981.

[5] P. Sen and C. J. Kim, "Microscale liquid-metal switches - A review," *IEEE Transactions on Industrial Electronics*, vol. 56, no. 4, pp. 1314-1330, April 2009.

[6] P. Sen and C. J. Kim, "A fast liquid-metal droplet microswitch using EWOD-driven contact-line sliding," *Journal of Microelectromechanical Systems*, vol. 18, no.1, pp. 174-185, February 2009.

[7] J. H. Chang et al., "Driving characteristics of the electrowetting-on-dielectric device using atomic-layer-deposited aluminum oxide as the dielectric," *Microfluid Nanofluid*, vol. 8, pp. 269-273, 2010.

[8] J. H. Chang, D. S. Kim, and J. J. Pak, ‘‘Simplified ground-type single-plate electrowetting device for droplet transport,’’ *Journal of Electrical Engineering & Technology*, vol. 6, no. 3, pp. 402-407, 2011.

[9] C. H. Chen and D. Peroulis, ‘‘Electrostatic liquid-metal capacitive shunt MEMS switch,’’ *IEEE MTT-S International Microwave Symposium Digest*, pp. 263-266, June 2006.

[10] O. Rezvanian et al., ‘‘Surface roughness, asperity contact and gold RF MEMS switch behavior,’’ *Journal of Micromechanics and Microengineering*, vol. 17, pp. 2006-2015, September 2007.

[11] J. Oberhammer and G. Stemme, ‘‘Active opening force and passive contact force electrostatic switches for soft metal contact materials,’’ *Journal of Microelectromechanical Systems*, vol. 15, no. 5, pp. 1235-1242, October 2006.

[12] S. T. Patton and J. S. Zabinski, ‘‘Fundamental studies of Au contacts in MEMS RF switches,’’ *Tribology Letters*, vol. 18, no. 2, pp. 215-230, February 2005.

[13] H. Kwon et al., ‘‘Investigation of similar and dissimilar metal contacts for reliable radio frequency Microelectromechanical Switches,’’ *Japanese Journal of Applied Physics*, vol. 47, no. 8, pp. 6558-6562, August 2008.

[14] S. T. Patton et al., ‘‘Lubrication of microelectromechanical systems radio frequency switch contacts using self-assembled monolayers,’’ *Journal of Applied Physics*, vol. 102, no. 2, July 2007.

[15] S. T. Patton et al., ‘‘Bimetallic nanoparticles for surface modification and lubrication of MEMS switch contacts,’’ *Nanotechnology*, vol. 19, August 2008.

[16] P. Sen and C. J. Kim, ‘‘A fast liquid-metal droplet switch using EWOD,’’ *IEEE MEMS 2007*, pp. 767-770, January 2007.

[17] M. D. Dickey et al., ‘‘Eutectic Gallium-Indium (EGaIn): A liquid metal alloy for the formation of stable structures in microchannels at room temperature,’’ *Advanced Functional Materials*, vol. 18, pp. 1097-1104, 2008.

[18] E. Colgate and H. Matsumoto, ''An investigation of electrowetting-based microactuation,'' *Journal of Vacuum Science & Technology. A*, vol. 8, no.4, pp. 3625-3633, July/August 1990.

[19] J. Lee and C. J. Kim, ''Surface-tension-driven microactuation based on continuous electrowetting,'' *Journal of Microelectromechanical Systems*, vol. 9, no. 2, pp. 171-180, June 2000.

[20] H. Moon et al., ''Low voltage electrowetting-on-dielectric,'' *Journal of Applied Physics*, vol. 92, no.7, pp. 4080-4087, October 2002.

[21] S. K. Cho, H. Moon, and C. J. Kim, ''Creating, transporting, cutting, and merging liquid droplets by electrowetting-based actuation for digital microfluidic circuits,'' *Journal of Microelectromechanical Systems*, vol. 12, no. 1, pp. 70-80, February 2003.

[22] Z. Wan, H. Zeng, and A Feinerman, ''Reversible electrowetting of liquid metal droplet,'' *Transactions of the ASME*, vol. 127, pp. 388-394, April 2007.

[23] J. K. Luo et al., ''Moving-part-free microfluidic systems for lab-on-a-chip,'' *Journal of Micromechanics and Microengineering*, vol. 19, April 2009.

[24] H. J. J. Verheijen and M. W. J. Prins, ''Reversible electrowetting and trapping of charge: Model and experiments,'' *Langmuir*, vol. 15, no. 20, pp. 6616-6620, September 1999.

[25] C. J. Kim and M. C. Wu, ''Electrowetting-based driving of liquid-metal droplet for reliable RF switching,'' *Airforce Research Laboratory Final Report* AFRL-VS-PS-TR-2005-1186, October 2005.

[26] C. H. Chen, J. Whalen, and D. Peroulis, ''Non-toxic liquid-metal 2-100 GHz MEMS switch,'' *IEEE MTT-S International Microwave Symposium Digest*, pp. 363-366, June 2007.

[27] L. Latorre et al., ''Electrostatic actuation of microscale liquid-metal droplets,'' *Journal of Microelectromechanical Systems*, vol. 11, no. 4, pp. 302-308, August 2002.

[28] Z. Wan, H. Zeng, and A. Feinerman, ''Area-tunable micromirror based on electrowetting actuation of liquid-metal droplets,'' *Applied Physics Letter*, vol. 89, no. 20, November 2006.

[29] R. C. Chiechi et al., ''Eutectic GalliumIndium (EGaIn): A moldable liquid metal for electrical characterization of self-assembled monolayers,'' *Angewandte Chemie Int Ed.*, vol. 47, pp. 142-144, 2008.

[30] T. Liu, P. Sen, and C. J. Kim, ''Characterization of liquid-metal Galinstan for droplet applications,'' *IEEE*, pp. 560-563, 2010.

[31] S. J. Mazlouman et al., ''A reconfigurable patch antenna using liquid metal embedded in a silicone substrate,'' *IEEE Transactions on Antennas and Propagation*, vol. 59, no. 12, pp. 4406-4412, December 2011.

[32] J. Simon, S. Saffer, and C. J. Kim, ''A liquid-filled microrelay with a moving mercury microdrop,'' *Journal of Microelectromechanical Systems*, vol. 6, no.3, pp. 208-216, September 1997.

[33] Y. Kondoh et al., ''High-reliability, high-performance RF micromachined switch using liquid Metal,'' *Journal of Microelectromechanical Systems*, vol. 14, no. 2, pp. 214-220, April 2005.

[34] J. Kim et al., ''A micromechanical switch with electrostatically driven liquid-metal droplet,'' *Sensors and Actuators A*, vol. 97-98, pp. 672-679, 2002.

[35] P. Sen and C. J. Kim, ''Electrostatic fringe-field actuation for liquid-metal droplets,'' in *Proceedings of The 13^{t}h International Conference on Solid-State Sensors, Actuators and Microsystems*, Seoul, Korea, pp. 705-708, June 2005.

[36] L. Minnema, H. A. Barneveld, and P. D. Rinkel, ''An investigation into the mechanism of water treeing in polyethylene high-voltage cables,'' *IEEE Transactions on Electrical Insulation*, vol. EI-15, no. 6, pp. 461-472, December 1980.

[37] G. Beni and S. Hackwood, ''Electrowetting displays,'' *Applied Physics Letter*, vol. 38, no. 4, November 1981.

[38] M. G. Pollack, A. D. Shenderov, and R. B. Fair, ‘‘Electrowetting-based actuation of droplets for integrated microfluidics,’’ *Lab Chip*, vol. 2, pp. 96-101, 2002.

[39] P. Sen and C. J. Kim, ‘‘A liquidsolid direct contact low-loss RF micro switch,’’ *Journal of Microelectromechanical Systems*, vol. 18, no. 5, pp. 990-997, October 2009.

[40] C. C. Cho, R. M. Wallace, and L. A. Files-Sesler, ‘‘Patterning and etching of amorphous Teflon films,’’ *Journal of Electronic Materials*, vol. 23, no. 8, pp. 827-830, 1994.

[41] DuPont Teflon AF Amorphous Fluoropolymer Product Information - Processing and Use.

[42] MicroChemicals Photoresist Processing Datasheet.